International Journal of Pharmaceutics 612 (2022) 121296

Contents lists available at ScienceDirect

International Journal of Pharmaceutics

journal homepage: www.elsevier.com/locate/ijpharm

Repurposing chlorpromazine for anti-leukaemic therapy by nanoparticle encapsulation

Edvin Tang Gundersen [a,b], Jan-Lukas Førde [a,c], Benedicte Sjo Tislevoll [d], Calum Leitch [d], Gillian Barratt [e], Bjørn Tore Gjertsen [d], Lars Herfindal [a,*]

[a] Centre for Pharmacy, Department of Clinical Science, University of Bergen, Bergen, Norway
[b] Hospital Pharmacies Enterprise, Western Norway, Bergen, Norway
[c] Department of Internal Medicine, Haukeland University Hospital, Bergen, Norway
[d] Centre of Cancer Biomarkers CCBIO, Department of Clinical Science, University of Bergen, Bergen, Norway
[e] Université Paris-Saclay, CNRS, Institut Galien Paris-Saclay, Châtenay-Malabry, France

ARTICLE INFO

Keywords:
Acute myeloid leukaemia
Drug repurposing
Chlorpromazine
Nanoparticles
PLGA

ABSTRACT

Treatment of acute myeloid leukaemia (AML) relies on decades-old drugs, and while recent years have seen some breakthroughs, AML is still characterised by poor prognosis and survival rate. Drug repurposing can expedite the preclinical development of new therapies, and by nanocarrier encapsulation, the number of potentially viable drug candidates can be further expanded. The anti-psychotic drug chlorpromazine (CPZ) has been identified as a candidate for repurposing for AML therapy. Nanoencapsulation may improve the suitability of CPZ for the treatment of AML by reducing its effect on the central nervous system. Using the emulsion-evaporation technique, we have developed PEGylated PLGA nanoparticles loaded with CPZ for AML therapy. The nanoparticles were characterised to be between 150 and 300 nm by DLS, of spherical morphology by TEM, with a drug loading of at least 6.0% (w/w). After an initial burst release of adsorbed drug, the remaining 80% of the drug was retained in the PLGA nanoparticles for at least 24 h. The CPZ-loaded nanoparticles had equal cytotoxic potential towards AML cells to free CPZ, but acted more slowly, in line with the protracted drug release. Crucially, nanoparticles injected intravenously into zebrafish larvae did not accumulate in the brain, and nanoencapsulation also prevented CPZ from crossing an artificial membrane model. This demonstrates that the purpose for nanoencapsulation of CPZ is fulfilled, namely avoiding effects on the central nervous system while retaining the anti-AML activity of the drug.

1. Introduction

Acute myeloid leukaemia (AML) is an aggressive hematopoietic stem cell disorder characterised by arrested differentiation, excessive proliferation, and rapid accumulation of myeloid precursors cells in the bone marrow (Longo et al., 2015). This results in impaired bone marrow function such as reduction of platelet-producing megakaryocytes (thrombocytes), red blood cells (erythrocytes), and myelocytic white blood cells (leukocytes), and the disease manifests as anaemia, bleeding, and impaired immune system with subsequent increased risk of life-threatening infections (Kohlschütter et al., 2008). The uncontrolled growth of AML cells also results in overpopulation of the bone marrow that eventually forces the AML blasts to enter the blood stream. AML is a heterogenous disease with large variations in differentiation status of the blasts, genetic aberrations, disease progression, response to treatment, and prognosis (Kohlschütter et al., 2008). It is the most common form of acute leukaemia in adults and incidence increases with advanced age, the median age of presentation being 67 years (Estey and Döhner, 2006).

AML is primarily treated with a combination of an anthracycline, daunorubicin (60–90 mg/m^2) or idarubicine (10–12 mg/m^2) for 3 days, and cytarabine (Ara-C) (200 mg/m^2) for 7 days ("3 + 7") (Rowe and Tallman, 2010; Dohner, 2010). While efforts have been made to improve the survival rate of AML patients with better cytostatic drugs and treatments, the "3 + 7" regimen remains the standard for induction therapy against AML more than 40 years after it was developed (Dohner, 2010; Rowe, 2013; Lichtman, 2013; Fernandez et al., 2009). For younger patients (under 65 years) with poor or intermediate risk,

* Corresponding author.
E-mail address: lars.herfindal@uib.no (L. Herfindal).

https://doi.org/10.1016/j.ijpharm.2021.121296
Received 12 July 2021; Received in revised form 26 October 2021; Accepted 11 November 2021
Available online 15 November 2021

allogeneic stem cell therapy may be considered, which achieves improved survival (Wahlin et al., 2002; Cornelissen, 2007).

There have been some advances in the therapy of AML, such as the tyrosine kinase inhibitor midostaurin targeting FLT3, enasidenib for advanced mutant IDH2 patients, the CD33 + antibody-drug conjugate gemtuzumab-ozogamicin given in conjunction with standard chemotherapy in AML, and the selective BCL-2 inhibitor venetoclax (Chen et al., 2019; DeStefano and Hourigan, 2018; Stone, 2017). Additionally, Vyxeos® (CPX-351) shows improved survival for adults with newly diagnosed high-risk AML such as therapy-related AML (t-AML) or AML with myelodysplasia-related changes (AML-MRC) (Administration, 2017; Chen et al., 2018; Blair, 2018). Vyxeos® is noteworthy as it is not a new drug, but a liposomal formulation of cytarabine and daunorubicin encapsulated at a fixed 5:1 ratio.

In response to the arduous process of traditional drug development, repurposing of drugs has become an attractive and efficient strategy to improve the therapy of several diseases (Jin and Wong, 2014; McCabe et al., 2015; Ashburn and Thor, 2004; Gupta et al., 2013; Andresen and Gjertsen, 2017). For example, the anti-emetic compound thalidomide was originally withdrawn due to its teratogenic properties but has, along with analogues, shown effectiveness against myelomas (Gupta et al., 2013; Andresen and Gjertsen, 2017; Ito and Handa, 2015; Steins et al., 2003). Similarly, chlorpromazine (CPZ), originally an anti-psychotic drug used to treat disorders such as schizophrenia, is identified as a potential treatment for AML (Sachlos, 2012; Haag, 2013) and other leukaemia subtypes (Zhelev et al., 2004). In addition, CPZ has also shown synergistic potential against cancers when given in combination with other anti-neoplastic drugs (Hanusova, 2015), and is recognised together with other phenothiazines for circumventing multidrug resistance in cancer cells (Michalak, 2006). However, CPZ easily crosses the blood–brain barrier (BBB) and affects the central nervous system (CNS), and in non-schizophrenic patients this results in negative side-effects like drowsiness, dizziness, and extrapyramidal reactions such as tremors, involuntary movements and twitching (Drug database; Drug database; Abidi and Bhaskara, 2003).

One method of preventing CPZ from affecting the CNS is by encapsulating the drug in a nanocarrier unable to cross the BBB. Nanoscale (<1000 nm) drug delivery systems have attracted immense interest and research activity in recent decades, due to their many potential benefits for drug delivery, such as reduced toxic side-effect, improved injectable dose, or improved therapeutic response (Pinto Reis et al., 2006; Parveen et al., 2012; Narvekar et al., 2014; Fonseca-Santos et al., 2015; Agrahari et al., 2016). Nanocarriers vary in composition, function, and characteristics, and can be made of natural or synthetic polymers, metal or metal oxides, or lipids (Svenson, 2014; Anselmo and Mitragotri, 2016; Wicki et al., 2015). The different materials all share the ability to transport molecules and alter the pharmacokinetic profile of the drug without changing the structure of the drug itself.

Drugs encapsulated in nanocarriers are also protected from rapid excretion in the kidneys or metabolism in the liver (Wicki et al., 2015; Solaro et al., 2010; Whitehead et al., 2009). This protection helps prolong the usually short half-lives of circulating drugs, improving the bioavailability of the drug and exposure of target cells. However, nanocarriers entering the blood stream will eventually be detected and degraded by macrophages of the mononuclear phagocytic system (MPS), particularly in the liver and spleen. This can be avoided by surface modification with the hydrophilic polymer PEG (poly(ethylene glycol) $[CH_2CH_2O]_n$). PEG not only prevents nanocarrier agglomeration by providing steric stabilisation, but also prevents their opsonisation and subsequent elimination by macrophages (Malam et al., 2009; Cheng et al., 2007; Suk et al., 2016). Composed of either natural or synthetic polymers, polymer-based nanocarriers are an attractive and extensively researched drug delivery platform (Kamaly et al., 2016; Nair and Laurencin, 2007; Uhrich et al., 1999), with many polymers being favoured for their biocompatibility and biodegradability (Nair and Laurencin, 2007; Makadia and Siegel, 2011). The most commonly used polymers for in drug delivery systems are the synthetic polyesters polylactide (PLA) and poly(D,L-lactide-co-glycolide) (PLGA) (Danhier et al., 2012; Dinarvand et al., 2011; Panyam and Labhasetwar, 2003), both of which are biocompatible, biodegradable, and FDA-approved (Sah et al., 2013; Athanasiou et al., 1996).

The present study was initiated based on the aim to repurpose CPZ for therapy against myeloid malignancies like AML. To avoid unwanted off-target effects on the CNS, CPZ was encapsulated in a nanoformulation which does not cross the BBB. We chose the PLGA nanoparticle platform since it has been used with success to encapsulate hydrophobic compounds. To find out if the nanoformulation prevented CPZ crossing BBB, we used an artificial membrane system, as well as zebrafish embryo to study nanoparticle biodistribution. The efficacy of free or encapsulated CPZ was studied in different AML cell lines, which represent the heterogeneity of the disease. Furthermore, in order to gain insight on nanoparticle-mediated drug delivery to AML cells, we studied the association and uptake of nanoparticles by flow cytometry and confocal microscopy. Taken together, our findings support the use of a nano-sized drug delivery platform in drug repurposing CPZ for AML therapy.

2. Materials and methods

2.1. Chemicals and reagents

Chlorpromazine hydrochloride (CPZ), formaldehyde, poly(vinyl alcohol) (PVA, Ave. $M_W = 10\,000$ g/mol), Nile Red (NR), tricaine (ethyl 3-aminobenzoate methane sulphonate), uranyl acetate (UA), was purchased from Sigma-Aldrich (St. Louis, MO, USA), and acetonitrile (ACN) and methanol (MeOH) from Merck KGaA (Darmstadt, Germany). Resomer® RG 505 Poly(D,L-lactide-*co*-glycolide) (PLGA, 50:50 lactide: glycolide, M_W = 54 000–69 000 g/mol) was purchased from Evonik Röhm Pharma GmbH (Essen, Germany). Resomer® PEG type RGP d 50105 Poly(ethylene glycol)-poly(DL-lactide-*co*-glycolide) (PLGA-PEG, 50:50 lactide:glycolide, $M_n = 50\,000$ g/mol for PLGA, $M_n = 5000$ for PEG) was purchased from Boehringer Ingelheim (Ingelheim, Germany). ProLong® Gold Antifade Mounting medium with DAPI, and Hoechst 33342 fluorescent DNA staining reagent was purchased from Thermo Fisher Scientific (Waltham, MA, USA). WST-1 cell proliferation reagent from Roche Diagnostics GmbH (Mannheim, Germany). Annexin V Alexa Fluor 647, propidium iodide (PI) and binding buffer, was purchased from Invitrogen (Carsbad, CA, USA). All other reagents were from Sigma-Aldrich and of analytical grade. E3 blue embryo water was provided by the Zebrafish facility at the Department of Bioscience, University of Bergen.

2.2. Nanoparticle preparation and characterisation

Nanoparticles consisting of PLGA or PLGA-PEG were prepared using the emulsion-evaporation technique (Halayqa and Domanska, 2014; Song et al., 1997; Quintanar-Guerrero et al., 1998). First, 50 mg polymer was dissolved in 2 ml chloroform. For CPZ- or Nile Red loaded nanoparticles, the organic phase was also added either 10 mg CPZ or 0.1 mg Nile Red. The organic solution was then mixed with a 10 ml PBS pH 9.5 with 1% w/v PVA. This mix was then immediately shaken, and vortexed for 1 min, followed by sonication for 1 min using a Misonix XL2020 sonicator (Farmingdale, NY, US) at 30 W output and intensity adjusted to 15–20%. The organic phase was removed by mild vacuum (gradually decreasing from 350 to 50 mbar) using a PC 3001 VARIO® vacuum pump (Vacuubrand GmbH & CO. KG, Wertheim, Germany) connected to a Laborota 4000 efficient rotary evaporator (Heidolph Instruments GmbH & CO. KG, Schwabach, Germany). The nanoparticle suspension was then washed twice by centrifugation for 10 min at 5500g, with resuspension in PBS pH 9.5 before a final resuspension in PBS pH 7.4 or pH 9.5. Nanoparticles were considered freshly prepared if used within 30 min of the final resuspension.

Size and zeta-potential characterisation of the nanoparticles was performed by dynamic light scattering (DLS) using a Zetasizer Nano ZS (Malvern Instruments Ltd., Malvern, UK) with Zetasizer Software version 7.10. For size analysis, the nanoparticles were diluted 1:50 in PBS in a semi-micro PS cuvette, analysed with "Multiple narrow modes (high resolution)" model, while for zeta-potential the nanoparticles were diluted 1:100 in MQ water in folded capillary cell cuvettes and analysed using "Auto mode" and Smoluchowski modelling.

For studies of size and morphology by transmission electron microscopy (TEM), copper grids coated with formvar film were gently placed on top of drops of nanoparticle solution for 60 s, film facing down, to transfer nanoparticles to the grid. The grid was washed by being placed on 5 subsequent drops of MQ for 5 s each, and finally on a drop of 2% w/v uranyl acetate for 10 s. Excess uranyl acetate was removed with absorbent paper, and the grids were left to dry for at least 30 min before imaging with a Jeol JEM-1230 transmission electron microscope (JEOL Ltd., Akishima, Japan).

2.3. Quantification of CPZ by liquid chromatography

The nanoparticles were analysed for drug content on the day of production. The nanoparticle suspensions were centrifuged at 4000*g* for 15 min, and the nanoparticle pellet resuspended and diluted in a 6:4 (v:v) ratio mix of ACN and MQ water. For other samples, the supernatant was diluted in a 6:4 (v:v) ratio mix of ACN:MQ.

The samples were injected into a Kromasil 100–5-C18 column (150 × 4.6 mm, Akzo Nobel, Sweden) connected to a Merck-Hitachi LaChrom HPLC system (VWR, Radnor, PA, USA) with a L-7100 pump, L-7200 autosampler, D-7000 interface, L-7455 diode array detector. The mobile phases were MQ (A) and ACN (B), both with 0.05% TFA. The HPLC gradient program started with the first 0.5 min at 40% A and 60% B, then an increase to 100% B during the next 3.5 min, followed by 1 min at 100% B. The gradient was then returned starting conditions over 1 min, and maintained at 40% A and 60% B for 2 min before next injection. The flow rate was 1.5 ml/min. Chromatograms were recorded at 306 nm and used for quantification of drug content with the HPLC System Manager software version 4.1. CPZ eluted as one sharp peak during 4.1 and 4.4 min with apex at 4.2 min. A standard curve ranging from 28 to 450 μM CPZ was used to calculate the CPZ content in the samples using interpolation from linear regression of the standard curve ($R^2 > 0.99$). Encapsulation efficiency (EE) and drug loading (DL) were calculated using Eqs. (1) and (2) respectively (Sauvage et al., 2018).

$$EE(\%) = \left(\frac{Amount\ CPZ\ in\ NC}{Amount\ CPZ\ added}\right) \times 100 \quad (1)$$

$$DL(w/w\%) = \left(\frac{Mass\ of\ CPZ\ in\ NC}{Total\ mass\ of\ NC}\right) \times 100 \quad (2)$$

2.4. In vitro drug release from nanocarriers

Immediately after production, drug-loaded nanoparticle suspensions were transferred to glass vials and either subjected to shaking on a Thermomixer Comfort (Eppendorf AG, Hamburg, Germany) at 400 RPM and 37 °C, or stored in fridge at 4 °C without shaking. The release media were PBS with pH 9.5 or 7.4 to see if physiological pH influenced CPZ release from the PLGA nanoparticles. Aliquots of 0.5 ml were sampled from the nanoparticle suspension, centrifuged at 4000*g* for 15 min to separate the nanoparticles from the supernatant, resuspended, and diluted in a 6:4 (v:v) ratio mix of ACN:MQ before HPLC.

2.5. Permeability assay

Assessment of membrane permeability was done on free and PLGA-encapsulated CPZ using the Corning® Gentest™ Pre-Coated PAMPA (parallel artificial membrane permeability assays) Plate System (Corning Inc., Corning, NY, USA) (Chen et al., 2008). The donor wells were filled with 0.3 ml of either free or PLGA-encapsulated CPZ in PBS pH 7.4 solution, while acceptor wells were filled with 0.2 ml of PBS pH 7.4. The assembled PAMPA plate system was then incubated according to the manufacturer's instructions, at room temperature without agitation for 5 h. These are the most commonly used conditions, and by using these, it is easier to compare our results with previously reported data. Samples from the donor and acceptor plates were collected and stored at −20 °C until analysis with HPLC. The drug concentration of each well was calculated from a standard curve, and permeability (P_e) was calculated using Eqs. (3) and (4) (Chen et al., 2008).

$$\frac{C_{eq} = [CD(t) \bullet VD + CA(t) \bullet VA]}{(VD + VA)} \quad (3)$$

$$P_e(cm/s) = \frac{\left(\frac{-ln(1-CA(t))}{C_{eq}}\right)}{\left(A \bullet \left(\frac{1}{VD} + \frac{1}{VA}\right) \bullet t\right)} \quad (4)$$

where A = filter area (0.3 cm^2), VD = donor well volume (0.3 ml), VA = acceptor well volume (0.2 ml), t = incubation time (seconds), CA(t) = compound concentration in acceptor well at incubation time, CD(t) = compound concentration in donor well at incubation time. Recovery was calculated based on the amount of CPZ added to the system, and the combined amounts found in the donor and acceptor well at the end of the experiment.

2.6. Cell lines, general maintenance, and experimental conditions

For cell culturing, the following culture media were used: RPMI for the human acute promyelocytic leukaemia cell line HL-60 (ATCC CCL-240) and human AML cell line MOLM-13 (ACC 554) (Matsuo et al., 1997; Quentmeier et al., 2003), IMDM for the human monocytic leukaemia cell line MV4-11 (ATCC, CRL-9591), and MEM alpha for the human AML cell line OCI-AML3 (ACC 582). All media were enriched with 10% foetal bovine serum (FBS), 20 mM of L-glutamine, 100 IU/ml penicillin and 0.1 mg/ml streptomycin. Patient primary AML cells were cultured in IMDM and with the same enrichment, but with 20% FBS. All cell culture media and supplements were acquired from Sigma-Aldrich (St. Louis, MO, US). The cells were cultured in a humidified atmosphere at 37 °C and 5% CO_2. Primary AML cells were acquired from patients at Haukeland University Hospital following informed consent in accordance with the Declaration of Helsinki. Approval was obtained from the regional Ethics Committee (REK Vest; http://helseforskning.etikkom.no; Norwegian Ministry of Education and Research, 2012/2245, 2012/2247). Information on age, FAB-classification, cytogenetics etc. for each patient is given in Supplementary Table S1.

The following drugs and concentrations were tested in combination with 10 μM CPZ on the AML cell line MOLM-13: bortezomib (3 and 9 nM), cisplatin (2 and 6 μM), cytarabine (2.5 and 5 μM), daunorubicin (90 and 140 nM), emetine (50 and 120 nM), and etoposide (1.3 and 1.8 μM). The cells were incubated with drugs at culture conditions, 37 °C and 5% CO_2, without agitation for 24 h and measured for viability with the WST-1 assay. Coefficient of drug interaction (CDI) was used as a measure of synergy and is determined by first finding the effect relative to control (R) of each drug alone and in combination, and using these values as shown in Eq. (5) (Zhao et al., 2014).

$$CDI = \frac{R_{Combination}}{R_{Drug1} \times R_{Drug2}} \quad (5)$$

The CDI value of a drug combination indicates a synergistic effect if significantly below 1, an additive effect if equal to 1, and an antagonistic effect if above 1, after one-sample *t*-test ($p < 0.05$). A CDI value below 0.7 is a clear sign of synergy (Soica, 2014).

To study the cellular uptake of nanoparticles, MOLM-13 cells at a 3.5

$\times 10^5$ cells/ml were incubated with 2% v/v concentration of nanoparticles loaded with Nile Red. At different time points, 200 μl cells were sampled, and washed twice by adding 1 ml PBS, centrifuging at 300*g* for 10 min, and removing 1 ml PBS. The cells were immediately thereafter analysed by flow cytometry using a FACS Accuri C6 flow cytometer (BD Biosciences, San Jose, CA, US) with the following settings: 488 nm laser, 585/40 nm filter, and fast fluidics (66 μl/min). Analysis of the data collected was done using the Accuri CFlow software version 1.0.227.4 (BD Biosciences, San Jose, CA, US). Events were gated for living cells on FSC and SSC scatter plot, then for singlets in FSC-H and FSC-A scatter plot, recording at least 10 000 events in gating for living cells. The median fluorescence intensity of these cells was then used to illustrate nanoparticle uptake. Non-linear regression analysis of uptake kinetics was done using the SigmaPlot software, version 9.01, (Systat Software, Inc., San Jose, CA, USA).

For imaging by confocal microscopy, cells were treated identical to those analysed with flow cytometry but after washing, they were resuspended in 1 ml of 2% formaldehyde in PBS pH 7.4. The cells were left in the dark at RT for at least 30 min before the fixative was replaced with PBS. Cells were then transferred onto glass slides using a Shandon Cytospin 3 centrifuge at 300*g* for 10 min and mounted using ProLong Gold mounting medium with DAPI. Imaging was done using a Leica TCS SP5 confocal microscope fitted with an HCX PL APO CS 63.0 × 1.40 OIL UV objective, and controlled with the Leica Application Suite software version 2.7.3 (Leica Microsystems GmbH, Wetzlar, Germany). A 488 nm Argon laser was used for excitation of the Nile Red fluorochrome, while a 405 nm UV laser was used for the DAPI-stained nuclei.

To evaluate the cytotoxic effects of CPZ and nanoparticles, cells were seeded in 96-well plates with a volume of 100 μl per well, at 3.5×10^5 cells/ml unless otherwise specified, and treated with various concentrations of either free CPZ, empty nanoparticles, CPZ-loaded nanoparticles, or combinations of cytostatics and CPZ. Cells were incubated without agitation at culture conditions, 37 °C and 5% CO_2, for 24 h before adding the WST-1 reagent and incubated for another 2 h before reading the absorbance of enzymatically converted WST-1 reagent using the Infinite M200 PRO microplate reader with the Magellan software version 7.2 (Tecan Group Ltd., Männedorf, Zürich, Switzerland). Absorbance wavelength and reference wavelength were set to 450 nm and 620 nm, respectively. Wells without cells and wells with only nanoparticles were used as background controls. Immediately after reading metabolic conversion of WST-1, each well was added 100 μl of 4% formaldehyde fix in pH 7.4 PBS with 0.01 mg/ml Hoechst 33342. The nuclear morphology of fixed and stained cells was studied using an Axiovert 200 M fluorescence microscope (Carl Zeiss AG, Oberkochen, Germany). Image analysis and processing was done using the FIJI image processing package, ImageJ version 1.52p (U. S. National Institute of Health, Bethesda, MD, USA) (Schindelin et al., 2012; Schneider et al., 2012; Rasband).

In evaluating the kinetics of CPZ-induced cell death, MOLM-13 cells were seeded in 12-well plates at 3.5×10^5 cells/ml. Cells were sampled at given time-points and fixed in 2% formaldehyde fix in pH 7.4 PBS with 0.005 mg/ml Hoechst 33342, and apoptotic nuclei were counted to determine cell death.

The induction of apoptosis of leukaemia cells exposed to CPZ was also quantified by flow cytometry following Annexin V and Propidium iodide (PI) staining. Cells were seeded in 24-well plates at 2.0×10^5 cells/ml and a volume of 1 ml per well, and after 24 h of incubation, transferred directly to flow tubes and pelleted by centrifugation at 300*g* for 5 min at 4 °C. Washing of cells was done twice with ice-cold PBS, and after final removal of PBS, the cells were resuspended in 100 μl of 1X Annexin Binding containing 1.5 μl of Annexin V Alexa Fluor 647 (Invitrogen) and PI (to a concentration of 1 μg/ml) and left to incubate for 15 min at RT in dark. Finally, 400 μl of 1X Annexin Binding Buffer was added to each tube. Samples were analysed on a Guava® easyCyte flow cytometer (EMD Millipore). The results were analysed either with the online analysis software Cytobank or with version 10.4.2 of the FlowJo software (FlowJo, LLC, Ashland, OR, USA). Events were gated for cells, then by Pacific Blue +/- and PI +/- quadrants which were based on staining controls. Values were adjusted for control samples.

2.7. Zebrafish larvae maintenance, nanocarrier injection, and confocal imaging

Biodistribution of fluorescent nanoparticles was studied using larvae of the zebrafish (*Danio rerio*) of the optically transparent *casper* line (White et al., 2008; D'Agati et al., 2017), which were obtained from the Zebrafish Facility of the Department of Biological Sciences, University of Bergen. Zebrafish larvae were kept in fresh E3 medium at 28.5 °C and anesthetised in a 0.7 mM tricaine solution before injection and during imaging. At two days post-fertilisation (dpf), or around the long-pec stage (48 h) of the hatching period (48–72 h) per Kimmel et al. (Kimmel et al., 1995), the larvae were injected with approximately 4 nl of nanoparticles into their posterior cardinal vein. The nanoparticles were freshly made and loaded with the Nile Red fluorochrome. The larvae were imaged on the day of injection (2 h post-injection) and on the following day (1 day post-injection) with an Andor Dragonfly 505 confocal microscope (Andor Technologies, Inc., Belfast, UK) fitted with a CFI Plan Apochromat Lambda 10X objective, 561 nm excitation laser, and 600/25 nm band pass filter. Fluorescence images of larvae are a Z-projection obtained by summation of overlying pixels in the confocal Z-stack, and are visualised in "Red Hot" mode, wherein higher fluorescence intensity is presented as a colour gradient ranging from red to white, representing fluorescence with low to high intensity, respectively. Image analysis and processing was done using the FIJI image processing package, ImageJ version 1.52p (U. S. National Institute of Health, Bethesda, MD, USA) (Schindelin et al., 2012; Schneider et al., 2012; Rasband, xxxx).

3. Results

3.1. CPZ exhibits cytotoxic activity towards AML cell lines

To verify its previously described anti-AML effect (Sachlos, 2012), CPZ was tested on the four AML cell lines HL-60, OCI-AML3, MOLM-13, and MV4-11, as well as blasts collected from bone marrow or peripheral blood of AML patients. CPZ induced a dose- and time-dependent decrease in metabolic activity in both the AML cell lines and the patient blasts (Fig. 1A–C). The calculated EC50 values for MOLM-13 cells were 38 μM and 16 μM after treatment with CPZ for 24 and 48 h, respectively (Fig. 1B), and 21 μM and 15 μM for blasts from patient P1 (Fig. 1C). The anti-AML activity of CPZ was further confirmed by the Annexin/PI apoptosis assay. These data were consistent with our measurement of metabolic activity (Fig. 1D and E).

The combination of different cytostatic drugs has become standard for chemotherapy in the treatment of many cancers, including AML. We therefore tested if CPZ could potentiate the effect of various anti-AML drugs in the MOLM-13 cell line. We found that the combination of either emetine (EME) or valproic acid (VPA) with CPZ was more efficient than either of the drugs alone (Fig. 2A and B). A summary of the drug combination effect (CDI, Eq. (5) in Section 2) is given in Fig. 2C. This shows that significant synergy was obtained with bortezomib (3 and 9 nM), daunorubicin (140 nM), emetine (120 nM), and valproic acid (1 and 1.5 mM). Emetine at 120 nM stood out as giving best synergistic response with CPZ, with a CDI of 0.55. Taken together, the data presented in Figs. 1 and 2 shows that CPZ has potential in AML treatment, particularly in combination with other anti-leukaemic drugs or drug candidates.

3.2. Nanoparticles show acceptable drug loading, size, and size distribution, and stability during cold storage

Encapsulation efficiency (EE) and drug loading (DL) were

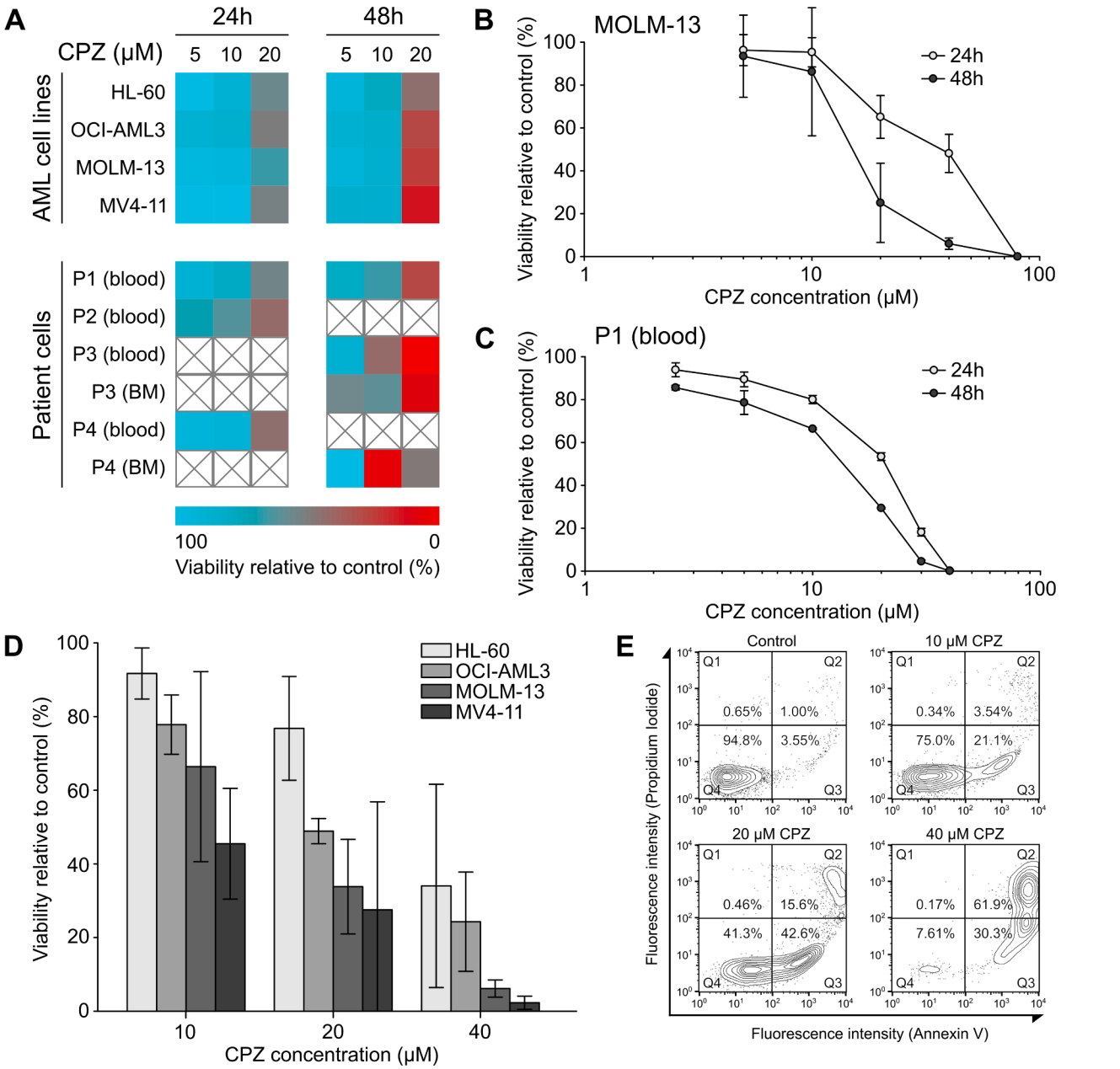

Fig. 1. CPZ shows dose-dependent cytotoxicity against AML cell lines and patient cells. (A): AML cell lines (HL-60, OCI-AML3, MOLM-13, and MV4-11) and AML patient cells (P1-4) derived from blood or bone marrow (BM) were incubated in growth conditions for 24 or 48 h with 5, 10, or 20 μM CPZ. Cells were tested for viability as measured by metabolic conversion of the WST-1 reagent, described in detail in the Methods section. CPZ dose–response curves of MOLM-13 cells and cells from blood of patient P1 are shown in (B) and (C) respectively. (D): AML cell lines incubated with 10, 20, or 40 μM CPZ for 24 h were tested for viability using Annexin/PI viability. (E): Flow cytometric dot plots of Annexin/PI viability assay of MOLM-13 cells. Cell were seeded to 2.0 × 10^5 cells/ml. All experiments were performed in triplicate.

determined by HPLC quantification of the CPZ in pelleted PLGA or PLGA-PEG nanoparticles. For both formulations, the average EE was around 37–38%, ranging from 26 to 51%, and the DL ranged from 4.1 to 8.6% (w/w), with an average of 6.3% (Table 1), obtained after analysis of 12 different production batches of each formulation.

CPZ-loaded nanoparticles were characterised with dynamic light scattering (DLS) for their Z-average size (d.nm) and Polydispersity Index (PdI). Results from three separate batches show that PLGA and PLGA-PEG nanoparticles had Z-average of 322 and 285 nm respectively, both with a PdI of around 0.150 (Fig. 3A and B, Table 1). In addition to being slightly smaller than PLGA, the PEGylated PLGA-nanoparticles were found to have a more negative Zeta-potential, at -15.7 mV compared with -4.8 mV for nonPEGylated nanoparticles (Table 1).

Measurements from TEM images showed a mean size of 165 ± 67 nm for PLGA and 139 ± 51 nm for PLGA-PEG (Table 1 and Fig. 3C and D). This was around half the size compared with the Z-average values found by DLS. Particle sizes measured by TEM ranged from 40 nm to 450 nm (Fig. 3C and D). The TEM images showed that the nanoparticles were spherical, with smooth and uniform surfaces (Fig. 3E–H).

Freshly made CPZ-loaded PLGA and PLGA-PEG were stored at 4 °C, and for 72 h monitored for size and drug loading (Fig. 4). In pH 7.4 PBS, both the PLGA and PLGA-PEG nanoparticles were stable, with diameters of around 320 nm and 280 nm, respectively, as measured by DLS (Fig. 4A). In pH 9.5 PBS however, PLGA-PEG maintained a stable diameter around 340 nm only for 24 h before increasing to around 400 nm after 72 h (Fig. 4B). Both formulations demonstrated similarly

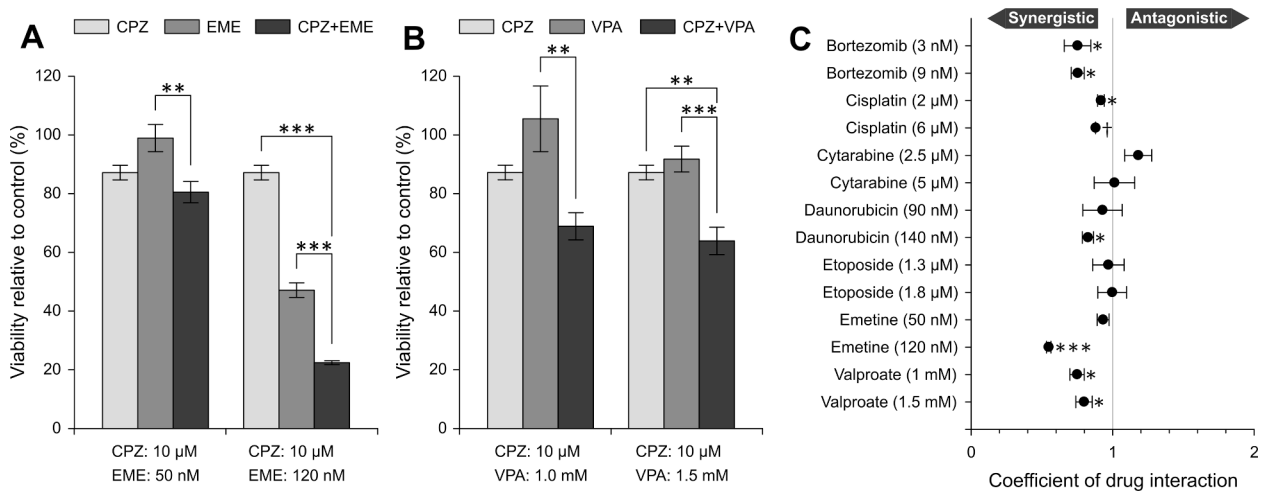

Fig. 2. CPZ exhibits synergistic activity with several anti-AML drugs. MOLM-13 cells were incubated for 24 h with CPZ (10 μM) alone, or with either EME (50 or 120 nM) (A) or VPA (1.0 or 1.5 mM) (B) and viability measured by metabolic conversion of the WST-1 reagent. (C): Coefficient of drug interaction (CDI) was calculated as described in the Methods section (see Eq. (5)). A CDI < 1 indicates synergism, a CDI = 1 indicates additivity, and a CDI > 1 indicates antagonism. Results are from a triplicate experiment. Asterisks *, **, and *** indicate $p \leq 0.05$, ≤ 0.01, and ≤ 0.001, respectively, from ANOVA Oneway (Bonferroni) statistical analysis (A,B) and one-sample two-sided t-test (C).

Table 1
Characterisation of CPZ-loaded PLGA-nanoparticles. The DLS and HPLC data are average of three and twelve separate production batches, respectively. EE and DL are average and standard deviation.

	DLS			TEM					HPLC	
	Z-average (d.nm)	PdI	Zeta pot. (mV)	Mean size (d.nm)	Median size (d.nm)	SD (d.nm)	Min. size (d.nm)	Max. size (d.nm)	Encapsulation efficiency[1] (%)	Drug loading (w/w %)[2]
PLGA	322	0.149	-4.8	165	148	68	67	454	38.1 ± 8.6	6.3 ± 1.4
PLGA-PEG	285	0.152	-15.7	139	130	51	42	367	37.0 ± 5.3	6.2 ± 0.9

1: Based on pellet concentration and total CPZ amount added.
2: Based on pellet concentration and total nanoparticle dry weight.

minimal drug release over time, with the ratio of CPZ located within the nanoparticles starting above 0.95 and remaining above 0.8 even after 72 h (Fig. 4C). From these data, the CPZ-loaded PLGA nanoparticles demonstrate stability for short-term cold storage with respect to size and drug loading.

3.3. Nanoparticle encapsulation prevents CPZ passively crossing membranes and readily associate with and are engulfed by AML cells

A critical step of repurposing CPZ to AML therapy is to restrict its ability to cross the BBB and exert effects on the CNS. Any potential nanocarrier intended to prevent BBB crossing of a drug should therefore be tested early in development for permeability. The Parallel Artificial Membrane Permeability Assay (PAMPA) was developed by Kansy et al. (1998), has been extensively used in early drug development to predict drug permeability (Avdeef, 2005), and is a reliable predictor of the BBB permeability of a drug (Di et al., 2003; Mensch et al., 2010; Bicker et al., 2014).

We used a PAMPA assay to measure the permeability (Pe) of free CPZ and CPZ encapsulated in either PLGA or PLGA-PEG nanoparticles (Fig. 5). The boundaries between the degrees of permeability is based on the work of Bennion et al. (2017), which classifies compounds as impermeable if log P_e < -6.14, low permeability when log P_e is between -6.14 and -5.66, medium permeability when log P_e is between -5.66 and -5.33, and high permeability when log P_e >-5.33. As a control of the system, the anthracycline daunorubicin was used. If membrane integrity is maintained, daunorubicin is impermeable, with a log P_e of -8.05 ± 0.45 (data not shown), which was the case in our experiments. The recovery was between 75 and 85%, with no apparent difference between free and nanoencapsulated CPZ, which could be due to a combination of adsorption of free CPZ or nanoparticles to the side or bottom of the wells, or CPZ residing in the membrane. Free CPZ exhibited a log P_e of -5.2, which indicates a high permeability. However, encapsulation of CPZ into either PLGA or PLGA-PEG reduced log Pe to around -6.1, which is on the boundary between low permeability and impermeable.

For the encapsulated CPZ to act on target cells, the nanoparticles must reach the cells and ideally be internalised, before the CPZ is released from the polymer matrix. To study this, cells were incubated with fluorescent PLGA or PLGA-PEG nanoparticles for up to 8 h and analysed by flow cytometry and confocal microscopy (Fig. 6). When incubated with 2% v/v concentration nanoparticles, flow cytometry showed a rapid increase in cell fluorescence, which reached a plateau after two hours for the PLGA-PEG nanoparticles. Cells treated with nonPEGylated nanoparticles showed increasing fluorescence intensity after eight hours. Moreover, PEGylation of the nanoparticles led to lower cellular uptake (Fig. 6A). The confocal images of MOLM-13 cells treated with 2% v/v of fluorescent nanoparticles showed that the nanoparticles appear to adhere to the cell membrane within 1 min of incubation (Fig. 6C, H). After 1 h of incubation, the amount of nanoparticles adsorbed onto the cell surface appeared to increase, though little to no change in overall appearance was observed between the 1-, 2-, and 8-hour samples (Fig. 6D–F, I–K). In some cases, nanoparticles were visible close to the nucleus (Fig. 6I and K).

3.4. CPZ retains its anti-AML effect when encapsulated in nanoparticles

We next wanted to know if nanoencapsulation of CPZ influenced its cytotoxic potential towards AML cells. MOLM-13 cells were therefore

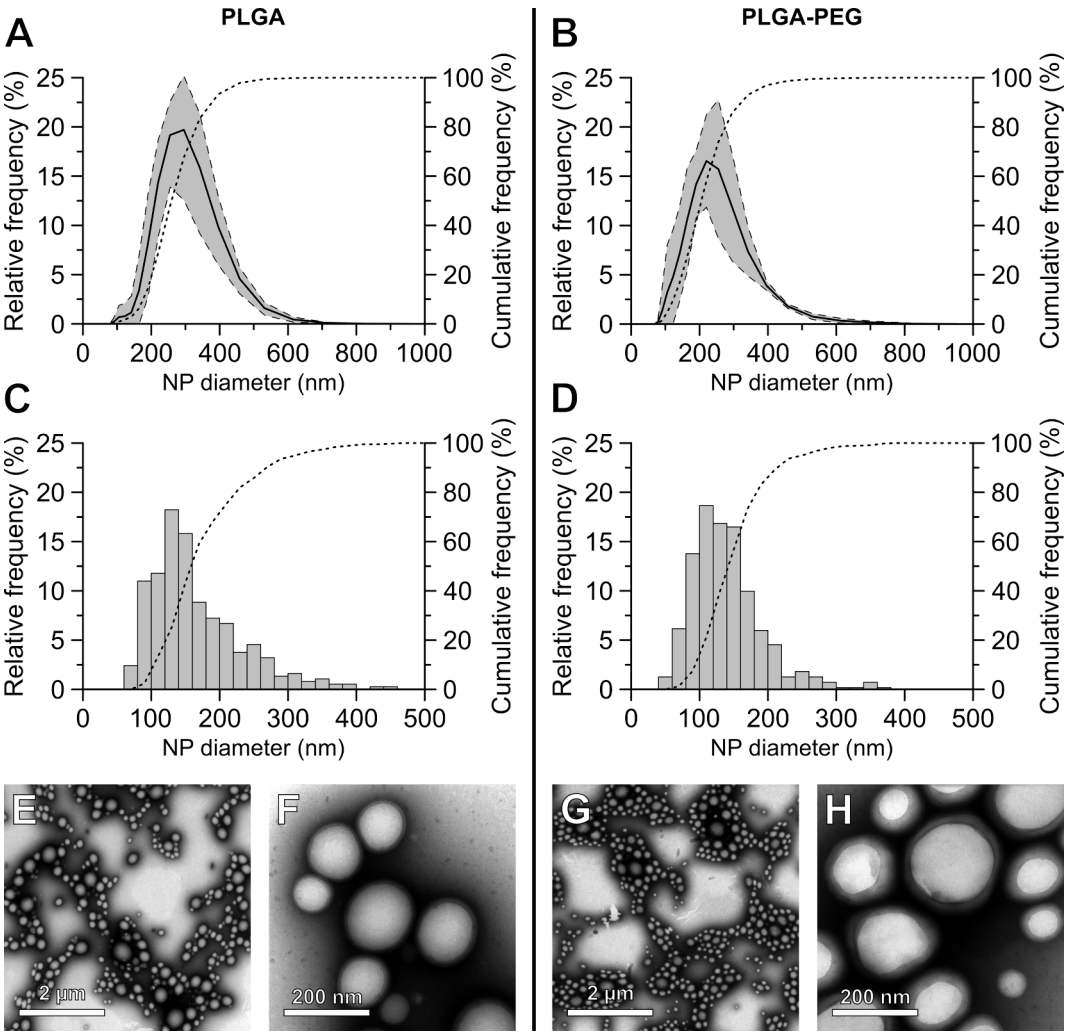

Fig. 3. Size distribution and morphology of CPZ-loaded PLGA and PLGA-PEG nanoparticles. (A,B): DLS measurements for the diameter of CPZ-loaded PLGA (A) and PLGA-PEG (B) nanoparticles. Each graph shows the average count-based distribution in size (d.nm) of three separate nanoparticle batches, analysed by DLS within 3 h of production. The dashed lines indicate the standard deviation and the dotted line represent the cumulative distribution. (C-H): Freshly prepared CPZ-loaded nanocarriers were stained with uranyl acetate and imaged with TEM. (C,D): Analysis of TEM images for the size distribution (d.nm) of nanoparticles made with PLGA (C) and PLGA-PEG (D). The dotted lines indicate the cumulative distribution frequency. TEM images are shown of CPZ-loaded PLGA (E,F) and PLGA-PEG (G, H). Scale bars represent either 2 µm (E,G) or 200 nm (F,H).

incubated with either free CPZ, or CPZ-loaded PLGA and PLGA-PEG nanoparticles for 24 h (Fig. 7). CPZ showed the same efficacy on MOLM-13 regardless of formulation, with 100% cell death at around 30 µM CPZ, and EC50 of 15 µM (Fig. 7A and B). The results also demonstrated that empty PLGA and PLGA-PEG nanoparticles were not cytotoxic, even after 24 h of incubation. Assessment of apoptosis based on cell nucleus morphology gave similar results to the WST-1 assay of metabolic activity (Fig. 7C and D).

3.5. Nanoparticles show limited drug release at physiological pH and delayed anti-AML activity

It is important to understand the drug release behaviour of nanoparticles, as this helps predict how the formulation will perform with regard to drug availability at the target site. Estimating nanoparticle drug loss during circulation, and thus CPZ concentration in blood, will help anticipate off-target effects and define the circulation time of the formulation. Freshly prepared CPZ-loaded PLGA and PLGA-PEG nanoparticles were incubated in pH 7.4 PBS and at 37 °C while gently shaken, and the amount of free and encapsulated drug analysed at different time-points (Fig. 8A and B). Immediately after adding the nanoparticles to the PBS, approximately 12% of the total CPZ was found to be free drug, both in PLGA and PLGA-PEG nanoparticle suspensions. Additionally, there was a marked release of CPZ from both nanoparticle types during the first hour of incubation, after which drug loading was stable for at least 24 h. After this, there was a gradual decrease of encapsulated CPZ in the PLGA-PEG nanoparticles over the next 28 days (Fig. 8B).

We next wanted to find if nanoencapsulation of CPZ affected the rate of apoptosis induction. MOLM-13 cells were incubated with free or nanoencapsulated CPZ, and the extent of cytotoxicity assessed at different time-points (Fig. 8C and D). Both CPZ-loaded PLGA and PLGA-PEG nanoparticles delayed the induction of cell death and the time to reach around 100% cell death. With PLGA, cell death of around 100% occurred after 8–12 h while this required only 6 h for free CPZ at an equivalent concentration (Fig. 8C). When comparing the time required to reach 50% cell death (t_{EC50}), free and PLGA-encapsulated CPZ took around 3 and 4.5 h, respectively. With PLGA-PEG, around 100% cell death was reached after 8 h while free CPZ at an equivalent well concentration only took 4 h (Fig. 8D). The t_{EC50} of free and PLGA-PEG-encapsulated CPZ was found to be around 2 and 3 h, respectively. Empty PLGA and PLGA-PEG nanoparticles of equivalent volumes to CPZ-loaded counterparts did not affect cell viability (open symbols in Fig. 8C and D).

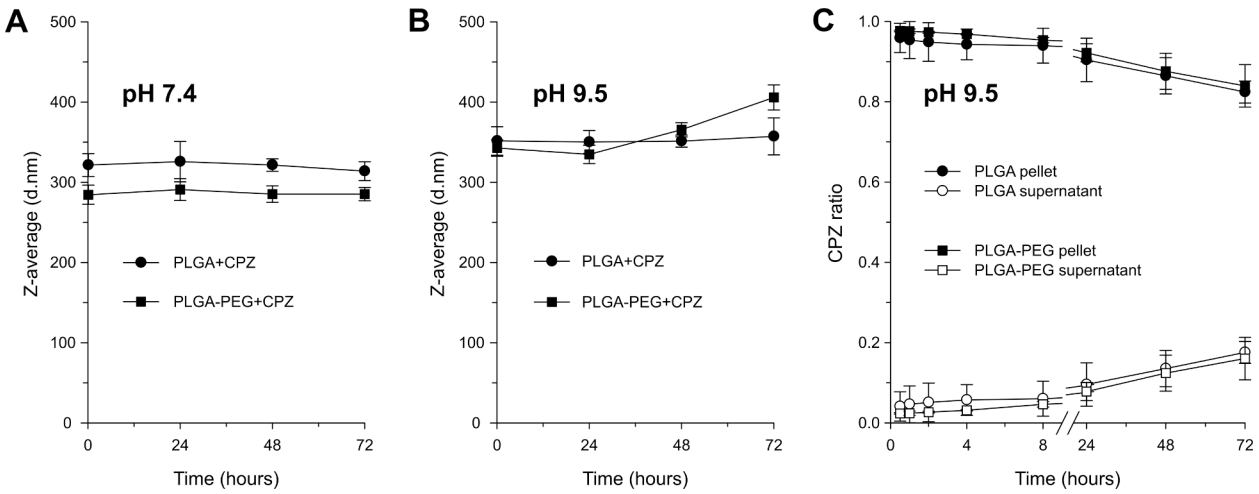

Fig. 4. Good shelf-life of nanocarriers is demonstrated by size stability and limited drug release. Freshly prepared batches of CPZ-loaded PLGA and PLGA-PEG were resuspended in PBS at pH 7.4 (A) or pH 9.5 (B,C), and kept at 4 °C in the dark and in sealed glass containers. Samples were taken at given time points and analysed for size (A,B) using DLS, and drug release (C) using HPLC as described in the Methods section. The release data represents the ratio of CPZ found in the pellet (nanoparticles) and supernatant (free form), after separation by centrifugation. The data show the average and standard deviation from three separate batches for each formulation.

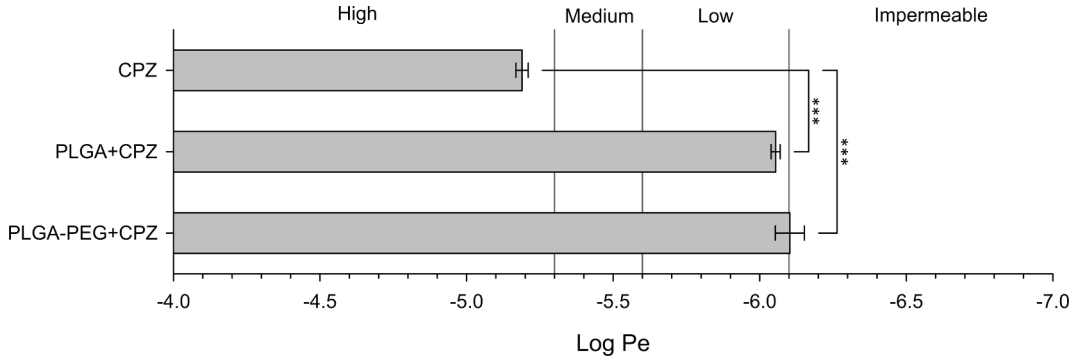

Fig. 5. Permeability of CPZ is significantly reduced by nanocarrier encapsulation. Free or encapsulated CPZ was diluted in pH 7.4 PBS and incubated in PAMPA plates for 5 h before analysis of CPZ well concentrations as described in the Methods section. Permeability (P_e) was calculated as described in the Methods section (see Eqs. (3) and (4)) and is provided as Log P_e. From one-way ANOVA with Bonferroni method, $p < 0.001$ (***) between free and encapsulated CPZ. No significant difference was found between PLGA and PLGA-PEG. The data are average and standard deviation of a triplicate experiment.

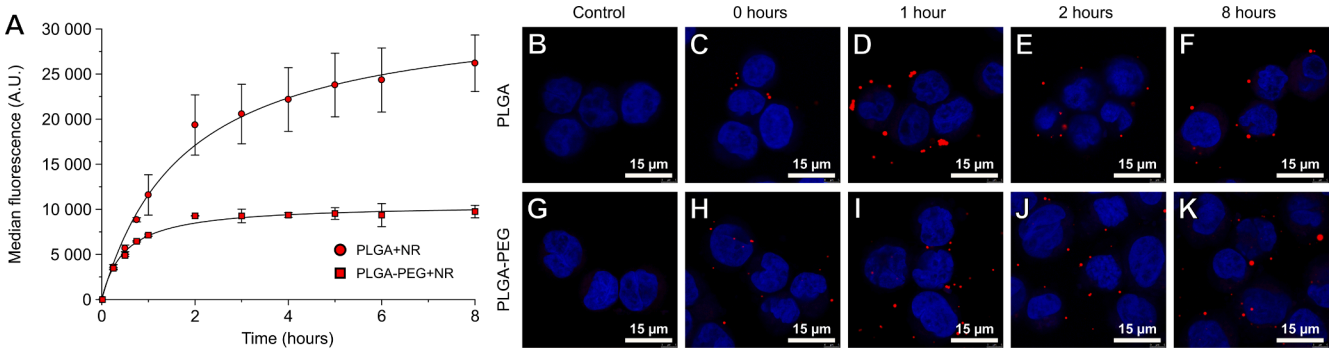

Fig. 6. PLGA-based nanoparticles rapidly associate with AML cells. MOLM-13 cells were incubated Nile Red-loaded nanoparticles at 2% v/v (A). After various times of incubation, cells were washed, and their fluorescence analysed with an Accuri C6 flow cytometer. The results are the average of median fluorescence, and standard deviation from a triplicate experiment. Non-linear regression curves were made using SigmaPlot, ver. 9.01, (Systat Software, Inc., San Jose, CA, USA). (B-K): Cells incubated with Nile Red-loaded nanoparticles were fixed in 2% buffered formaldehyde (in pH 7.4 PBS containing Hoechst 33342) and imaged with confocal microscopy. The scale bars in the confocal micrographs represent 15 µm. See Supplementary Figure S1 for gating strategy.

3.6. Nanoparticles injected in zebrafish larvae do not cross the BBB

In order to study the biodistribution of the nanoparticles, we injected PLGA or PLGA-PEG nanoparticles loaded with Nile Red into the caudal vein of zebrafish larvae aged 48 h post fertilisation, at the long-pec stage as described by Kimmel et al. (1995). Both PLGA and PLGA-PEG was

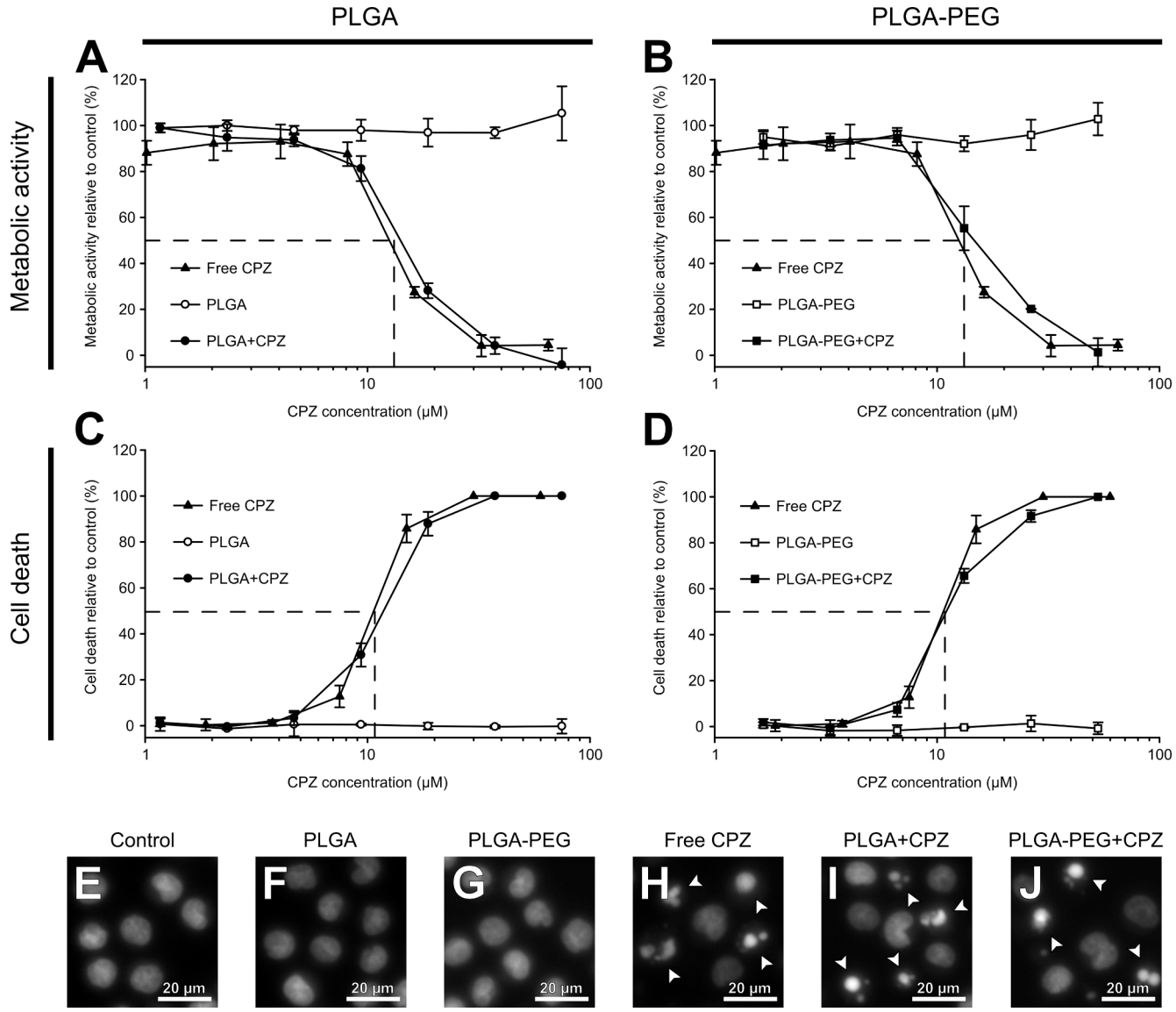

Fig. 7. CPZ-loaded PLGA nanoparticles have equal cytotoxicity towards AML cells compared to free CPZ. MOLM-13 cells were incubated for 24 h with various concentrations of either free CPZ, empty or CPZ-loaded nanoparticles. (A,C) are data with PLGA nanoparticles, and (B,D) are with PLGA-PEG nanoparticles. The cells were incubated with the different additions for 24 h before their viability relative to control was measured by the metabolic conversion of the WST-1 reagent. Following the plate reading for WST-1, the cells were fixed in 2% buffered formaldehyde (in pH 7.4 PBS containing Hoechst 33342). Using fluorescence microscopy, cells were counted for apoptosis and adjusted for control. The data in A-D are the averages and standard deviations from triplicate experiments. (E-J): Fluorescence microscopy images of Hoechst-stained nuclei of cells after 24 h of the different treatments. Arrows indicate typical apoptotic cells. Scale bars represent 20 μm.

present in the blood two hours post injection, although we could also observe some extra-vascular aggregations, particularly in the larvae injected with PLGA nanoparticles (Fig. 9C). The fluorescence intensity in the vasculature of the larvae two hours post injection was higher in the larvae injected with PLGA-PEG (Fig. 9E) compared to those injected with PLGA nanoparticles (Fig. 9C). The larvae were also imaged at 1 day post-injection. Here, PLGA nanoparticles could not be observed in the circulation, and instead appeared in the extravascular tissues, particularly in the ventral caudal region, and close to the duct of Cuvier (Fig. 9D). The PLGA-PEG nanoparticles were still present in the blood, although there were considerable amounts in the extravascular tissues as well (Fig. 9F). We did not observe any fluorescence in the brain or other parts of the central nervous system of larvae injected with either nanoparticle type (Fig. 9C-F). Zebrafish larvae injected with suspension media without nanoparticles did not show any fluorescence, except at the caudal-most part of the yolk extension, close to the injection site. This could be autofluorescence from the yolk, or due to tissue damage caused by the pressure during injection (Fig. 9A). This fluorescence was weaker in intensity one day post injection (Fig. 9B). We did not observe any toxic effects of the nanoparticles, nor any apparent damage to the larvae after injection.

4. Discussion

Treating AML remains a challenge due to poor overall disease prognosis, which has not been resolved by the new drugs that have been launched during the last decade (DiNardo and Wei, 2020). Our goal was to explore if the anti-psychotic drug CPZ could be repurposed for AML therapy, and by nanocarrier encapsulation, create a CPZ formulation unable to cross the BBB and cause CNS side effects.

CPZ showed cytotoxic potential in all cell lines tested, including the poor-prognosis cell line OCI-AML3 which has a complex karyotype, as well as in blasts isolated from AML patients, of which two, P1 and P3, were classified within the “adverse” risk category (see Supplementary

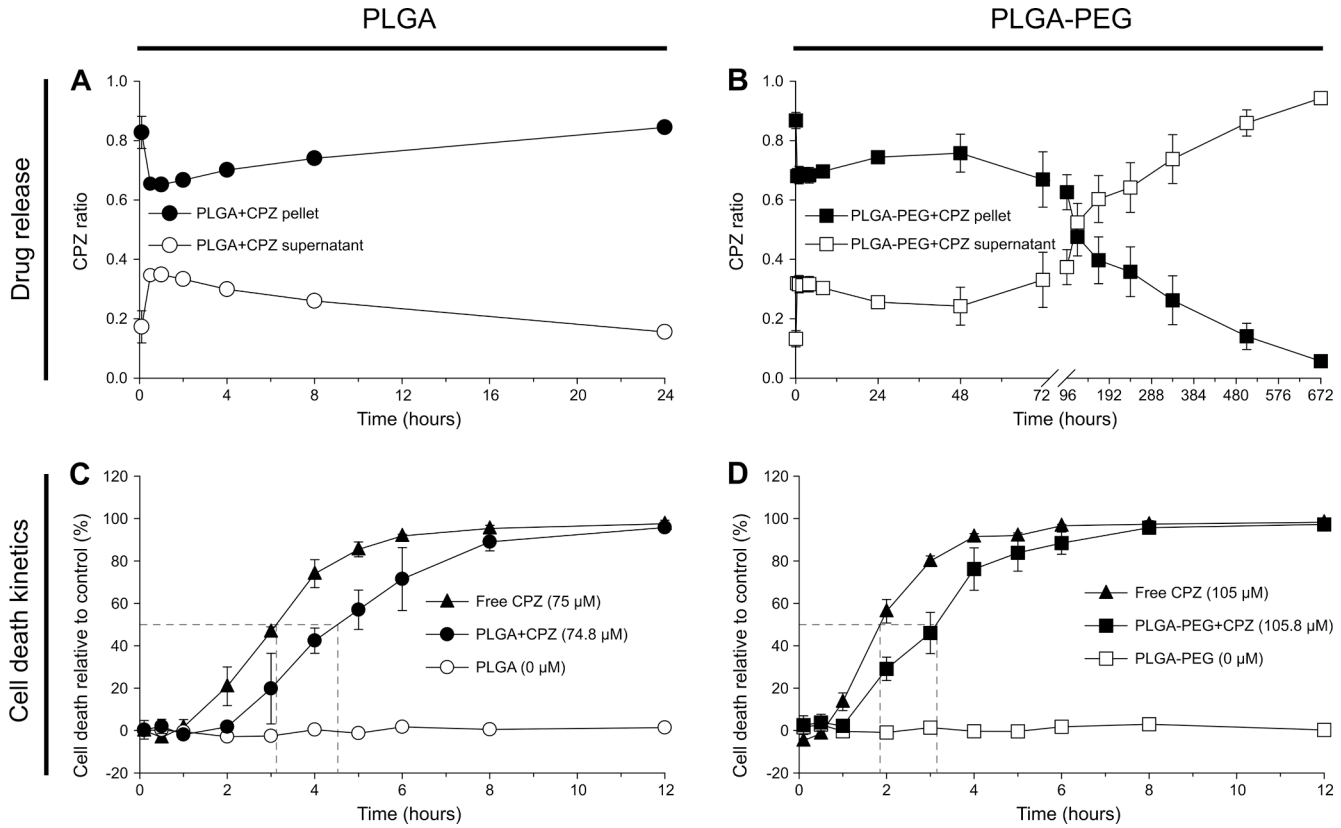

Fig. 8. CPZ-loaded PLGA/PLGA-PEG show quick but limited burst release at physiological pH and delayed cell death kinetics. Freshly prepared batches of CPZ-loaded PLGA (A) and PLGA-PEG (B) were resuspended in pH 7.4 PBS and stirred at 400 RPM and at 37 °C. Aliquots were sampled at given time-points and analysed for CPZ-content by HPLC as described in the Methods section. The release data represents the ratio of CPZ found in the pellet (nanoparticles) and supernatant (free form), after separation by centrifugation. (C, D): MOLM-13 cells were incubated for up to 12 h with 10% v/v concentration of either empty or CPZ-loaded PLGA (C) or PLGA-PEG (D) nanoparticles, or free CPZ of equivalent drug concentrations. At given time points aliquots were transferred to 2% buffered formaldehyde (in pH 7.4 PBS containing Hoechst 33342). Nuclei-stained cells were imaged with an Axiovert 200 M fluorescence microscopy and normal and apoptotic nuclei were counted. Data are from a triplicate experiment.

Table S1) (Dohner, et al., 2017). Additionally, CPZ synergised with bortezomib, daunorubicin, emetine, and valproate (Fig. 2), with emetine showing the greatest synergistic potential. These findings are important, since most chemotherapy, including those for AML, rely on drug combinations. Protein synthesis inhibitors have been shown to potentiate the effect of daunorubicin against AML cells *in vitro* and *in vivo* (Gausdal, et al., 2008), also when the drugs were co-loaded in liposomes (Myhren et al., 2014). Valproate, an inhibitor of histone deacetylase, also showed synergistic potential with CPZ and has previously been identified as a candidate for combination therapy in AML (Leitch et al., 2016; McCormack et al., 2012).

However, as CPZ is more effective with longer exposure time (48 vs 24 h of incubation, Fig. 1A–C), the drug presents a challenge with its highly variable half-life (between 2 and 60 h) and potential adverse effects on the central nervous system (MIDHA et al., 1989; McClelland et al., 1990). We found that CPZ at concentrations between 6 and 30 μM efficiently eradicated AML cells *in vitro*. The plasma-concentrations of CPZ in patients under treatment for acute psychosis are in the range from 8 to 80 ng/ml, equivalent to 0.025-0.25 μM (Kolakowska, 1976; Kolakowska et al., 1979; Wode-Helgodt and Alfredsson, 1981). It is therefore also important to minimise the level of free CPZ in the plasma to avoid effects on the CNS for use in AML therapy.

We developed a nanoformulation of CPZ wherein the drug is loaded within a matrix of PLGA nanoparticles. Although higher drug loading has been reported by Halayqa and Domanska (2014), our key rationale for the nanoencapsulation of CPZ is to avoid rapid release of the drug to avoid CNS affection.

We found that the drug release was less than 35% during the first hour (Fig. 8), after which the release of free drug could be attributed to the degradation of the nanoparticles. In line with this, the transfer of CPZ between the two compartments in the PAMPA assay was minimal if CPZ was encapsulated in either PLGA or PLGA-PEG nanoparticles compared with the free drug (Fig. 5). This suggests that encapsulation of CPZ in PLGA-based nanoparticles prevents passive diffusion of the drug through membranes which again could be an efficient method to avoid CNS-exposure of the drug. The release profile of CPZ-loaded PLGA nanoparticles by Halayqa et al. showed an initial burst release of 90% of the loaded CPZ occurring between 6 and 32 h depending on the PLGA concentration (w/v). While our nanoparticles also undergo burst release of CPZ at first, only 40% is released during the first 24 h. The slow release of CPZ from our nanoparticles compared to those of Halayqa et al. could be due to both a lower drug loading, but also a larger particle size. Larger particles will have less surface-to-volume ratio, which is beneficial in drug retention in nanoparticles. For potential AML therapy, it is important that the CPZ is retained inside the nanoparticles until the bone marrow is reached, in order to prevent off-target effects on the central nervous system.

The burst release was higher at pH 7.4 (Fig. 8A and B), compared to pH 9.5 (Fig. 4C). At pH 9.5, CPZ is estimated to be uncharged, however, after the initial burst release at pH 7.4, the release of CPZ similar to that seen at pH 9.5. It is likely that the burst release is due to surface-adsorbed CPZ-molecules being affected by the pH, whereas drug presented inside the nanoparticle is well retained. This is in line with other studies reporting that release rate is diffusion-controlled during early stage and erosion-controlled during the final stage (Fredenberg et al., 2011). From this, we may not expect further drug release until the

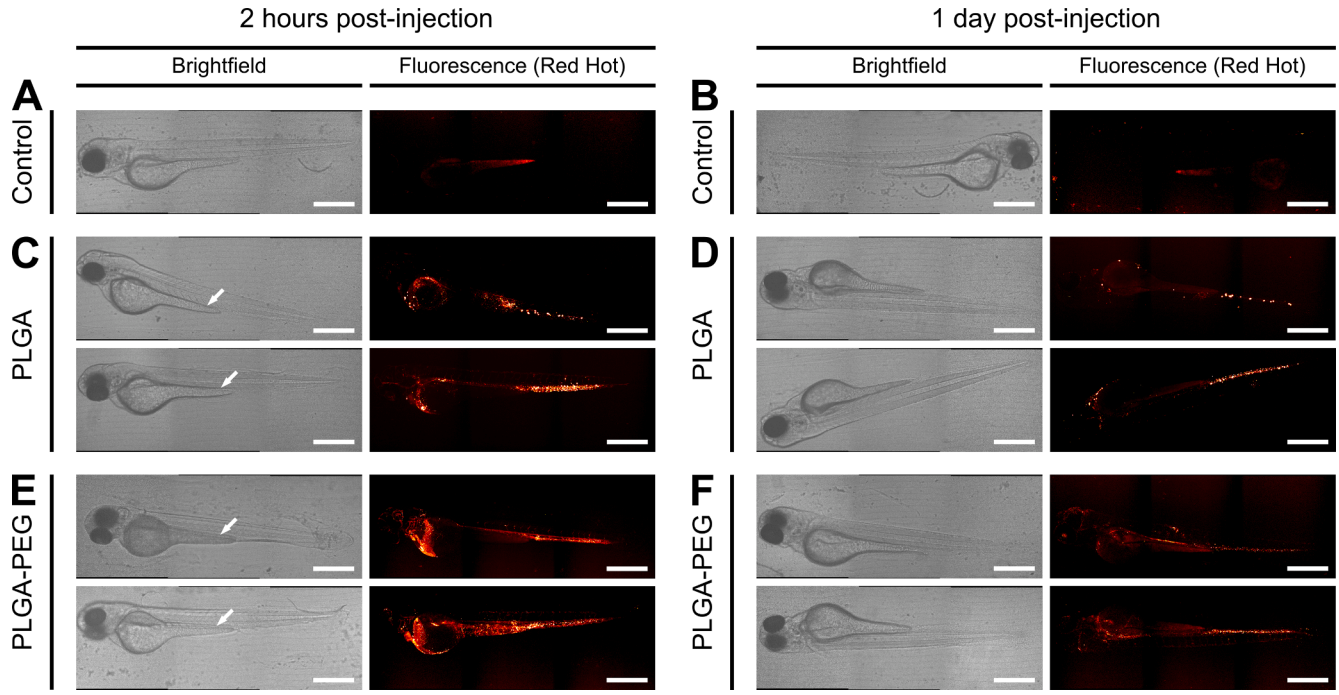

Fig. 9. Injected nanoparticles do not cross the BBB of zebrafish larvae. Zebrafish larvae were injected with 4 nl nanoparticles of PLGA (C,D) or PLGA-PEG (E,F), loaded with Nile Red fluorochrome. Injections were done into the posterior cardinal vein (indicated by arrows) on larvae aged 2 days post-fertilisation. Imaging was done with confocal microscopy 2 h and 1 day post-injection. Fluorescence images of larvae (A-F) are Z-projections obtained by summation of overlying pixels in the confocal Z-stack, and is shown in "Red hot" mode, where the fluorescence signal is gradient coloured by its intensity, ranging from red (low) to white (high). Scale bars represent 500 μm.

nanoparticles enter for instance the leukaemic bone marrow, which has a hypoxic and acidic environment (Thing Mortensen et al., 1998). However, as our cytotoxicity data shows, AML cell death occurs at equal concentrations for free and encapsulated drug (Fig. 7), and only between one and two hours delayed if encapsulated (Fig. 8C and D).

TEM measurements gave a lower size estimate compared with DLS (Table 1 and Fig. 3). The fact that DLS measures the hydrodynamic radius instead of the physical radius as with TEM is unlikely to account for this size difference. The presence of aggregates in the DLS samples could be the explanation, but we did not observe aggregates in the TEM samples, though TEM images may not be sufficient in distinguishing individual nanoparticles from aggregates. It could also be that smaller nanoparticles more easily adsorb to the grid while larger nanoparticles sediment. The Z-average of the nanoparticles did not change notably during cold storage (4 °C) for up to 72 h (Fig. 4A and B), indicating that aggregation or degradation did not occur. The size range between 30 and 300 nm for most of the nanoparticles is considered acceptable for intravenous delivery (Ferrari et al., 2018). In line with this, we did not notice blockage of blood vessels in zebrafish injected with the nanoparticles (Fig. 9).

While accumulation of nanoparticles in solid tumours due to the enhanced permeability and retention (EPR) effect is well described, a similar process in the leukaemic bone marrow is not properly documented. In normal bone marrow, the endothelium is continuous with a fenestrated basal membrane (Moghimi, 1995), and uptake of nanoparticles is by through transcytosis (Sahay et al., 2010; Sarin, 2010). Large particles are less prone to transcytosis compared to smaller (<80 nm) (Awasthi et al., 2003), reviewed in (Sauvage et al., 2015), but liposomes can be modified to enhance uptake despite large size (up to 200 nm) (Sou et al., 2007). The ability of our nanoparticles to home to the bone marrow has not been investigated, and biodistribution studies in leukaemic animals such as mice are needed to clarify this. Surface modification such as those used by Sou and co-workers (Sou et al., 2007), or other ligands targeting the bone marrow (Singh et al., 2019), could be used to enhance bone marrow targeting. However, there is considerable remodelling of the vascular niche in leukaemic patients for instance by transendothelial migration of blasts (Kumar and Chen, 2018; Duarte et al., 2018), which is likely to influence for instance passive transport of nanoparticles through the endothelium.

As demonstrated by metabolic assays (Fig. 7A and B) and verified by microscopy (Fig. 7C and D), PLGA-encapsulated CPZ is equally cytotoxic to free CPZ against the MOLM-13 cell line after 24 h. This was true regardless of both CPZ concentration and PEG inclusion. The PLGA or PLGA-PEG did not contribute to the cytotoxicity from CPZ-loaded nanoparticles, as demonstrated by lack of cytotoxicity of unloaded nanoparticles after 24 h (Fig. 7). It thus appears that the nanoparticles can deliver CPZ to the AML cells, to the same extent as the free drug.

From the flow cytometric results of fluorescent nanoparticles, it appears that the nanoparticles quickly either undergo cellular uptake into, or adherence onto, the MOLM-13 cells (Fig. 6A). The PLGA nanoparticles reached uptake saturation at around 8 h, while for PLGA-PEG nanoparticles it only took 2 h, though at a lower fluorescence intensity. This is as expected, since PEGylation of nanoparticles is known to reduce non-specific uptake by cells (Rabanel et al., 2014). Confocal microscopy showed that the nanoparticles were located along the cellular surface, and few were observed inside the cells (Fig. 6B–K). This could suggest that the nanoparticles are not internalised, and that the increase in cellular fluorescence shown by flow cytometry is primarily due to attachment to the cell membrane. However, one cannot exclude the possibility that the flow cytometry detects fluorescent signals which are not detectable in the confocal images.

Despite the differences in uptake between PLGA and PLGA-PEG, both formulations showed similar cytotoxicity across CPZ concentrations (Fig. 7). Judging from the release experiments (Figs. 4 and 8), the amount of free CPZ escaping from PLGA or PLGA-PEG (around 40%) was too low to be able to induce cell death, and we conclude that delivery of CPZ to the cells is mediated through the nanoparticles.

One explanation to the high efficacy of the nanoparticles, despite the

limited uptake, can be diffusion of drug in the interface between the nanoparticles and the cell membrane. Due to the low molecular weight and amphiphilic nature of CPZ, it will rapidly enter the cells as free form, as evidenced by the PAMPA assay (Fig. 5). Xu et al. disputes the general assumption that PLGA nanoparticles are taken up by endocytosis and release drug intracellularly, and instead argues for the possibility that cargo is delivered to cells by extracellular drug release and/or direct drug transfer to contacting cells (Xu et al., 2009). Both internalisation of CPZ via nanoparticles, or by diffusion can explain the delayed cytotoxic response (Fig. 8C and D), but also the high efficacy at 24-hour incubations (Fig. 7A-D), where the critical intracellular level for cytotoxic response apparently is reached.

The finding that the nanoparticles adhere to the cell membrane, rather than undergo cellular internalisation, is not necessarily problematic. Instead, cell surface adherence could be a preferable method of "presenting the drug" to the cells. By not relying on endocytosis for anti-AML effect of nanoparticles, the ability of CPZ to inhibit clathrin-dependent endocytosis is made irrelevant (Rejman et al., 2004; Dutta And Donaldson, 2012), as is the slowing effect of high PEGylation has on cellular uptake, which is included to prevent opsonisation (Rabanel et al., 2014; Walkey et al., 2012). Furthermore, if targeting ligands are included on the nanoparticles, they would only need to recognise and bind to AML cells, and not also facilitate uptake.

In zebrafish larvae, the PLGA-PEG nanoparticles were still present in the blood of the larvae at 24 h after injection (Fig. 9F). The PLGA nanoparticles were present in extravascular cells, presumably macrophages, especially in the caudal region (Fig. 9D), corresponding to the caudal haematopoietic tissue (Rosowski, 2020). The positive effect of PEGylation on circulation time in zebrafish larvae has been demonstrated for liposomes (Evensen et al., 2016). This could not be explained by cellular uptake of Nile Red or nanoparticles, since the fluorescence were evenly present in the vasculature. In addition, we noted some spots with high-intensity fluorescence, which could be aggregates of the nanocarriers circulating in the blood, or nanoparticles engulfed by circulating leukocytes. The zeta-potentials of the CPZ-loaded PLGA and PLGA-PEG nanoparticles were around -4.8 and -15.7 mV, respectively. Neutral or negative nanoparticles favour longer circulation half-life as they reduce serum protein adsorption (Alexis et al., 2008). Judging from our findings in zebrafish larvae, PEGylation and a more negative zeta-potential is beneficial for increased circulation time of the nanoparticles.

The lack of fluorescence inside the brain, or in the brain endothelium (Fig. 9C-F), indicates that there was no active or passive transport of nanocarriers through the BBB. This shows that the main purpose of the nanoparticles is fulfilled, namely, to prevent drug accumulation in the CNS. Indeed, while the BBB of the zebrafish is said to be fully developed at 10 dpf, its maturation starts at 3 dpf and already then shows functionality and size-dependent exclusion of large MW particles of above 4 kDa (Fleming et al., 2013; White et al., 2019). This is more than sufficient for our nanoparticles, and as the BBB of ZF larvae are similar to those of mammals in both structure and function such as compound-specific permeability (Fleming et al., 2013; White et al., 2019), it can provide results that are relevant for the BBB functionality of humans (Quiñonez-Silvero et al., 2020).

Provided that the drug release in the blood of zebrafish larvae is similar to that presented at pH 7.4 PBS (Fig. 8A and B), we conclude that nanoencapsulation of CPZ can be used to prevent crossing of the BBB, and also increase circulation time of the drug, lowering the distribution volume, and reducing potential off-target effects.

5. Conclusion

Adequate treatment of AML remains a challenge and to resolve this, new and improved therapies need to be developed. Following the concept of repurposing, we have verified the efficacy of CPZ towards AML cells, and developed a nanoformulation of CPZ which retains cytotoxicity towards AML cells. Importantly, the nanoformulation does not cross the BBB, which is a requirement for the use of CPZ in cancer therapy. Since our nanoparticles do not require cell uptake to function, further modifications with PEG-conjugated surface ligands are not needed to facilitate drug delivery. However, ligands that increase drug delivery to AML cells relative to other cell types can increase target specificity and further minimise unwanted off-target effects. Furthermore, ligands that directs the nanoparticles to the bone marrow microenvironment and leukaemic stem cells could also enhance their usefulness in consolidation therapy of AML (Singh et al., 2019). We believe that drug repurposing by nanocarrier encapsulation has an important role in supporting future breakthroughs in AML therapies, and that as a proof-of-concept, our CPZ-loaded PLGA-based nanoparticles demonstrate this. Further evaluation of the efficacy towards AML cells, and perhaps equally important, the ability of nanoparticles to prevent off-target effects from CPZ on the central nervous system, should be done in an *in vivo* model. Using rodents like mice transplanted with human AML cells, it is possible to monitor development of the disease non-invasively using imaging techniques (Gelebart et al., 2015), and at the same time detect, for instance, changes in motor-effects caused by CPZ crossing the BBB. Importantly, it will also reveal to what extent our nanoparticles accumulate in the leukaemic bone marrow, which is the ultimate target for AML therapy.

CRediT authorship contribution statement

Edvin Tang Gundersen: Conceptualization, Data curation, Formal analysis, Investigation, Methodology, Validation, Visualization, Writing – original draft, Writing – review & editing. **Jan-Lukas Førde:** Investigation, Methodology, Visualization, Writing – original draft. **Benedicte Sjo Tislevoll:** Investigation, Data curation. **Calum Leitch:** Investigation, Writing – review & editing. **Gillian Barratt:** Conceptualization, Supervision, Writing – review & editing. **Bjørn Tore Gjertsen:** Conceptualization, Funding acquisition. **Lars Herfindal:** Conceptualization, Funding acquisition, Investigation, Methodology, Project administration, Resources, Supervision, Writing – original draft, Writing – review & editing.

Declaration of Competing Interest

The authors declare that they have no known competing financial interests or personal relationships that could have appeared to influence the work reported in this paper.

Acknowledgements

This work was funded by grants from the Western Norway Health Authorities to ETG (grant no.: 912122), LH (grant no.: 912052) and JLF (grant no.: F-12533), and the Norwegian Cancer Society (grant no.: 206696), and the Norwegian Society for Children's Cancer to LH. CL, BST and BTG were supported by funding from the Norwegian Cancer Society with Solveig & Ole Lunds Legacy, Øyvinn Mølbach-Petersens Fund for Clinical Research and grant no 303445. Additionally, CL, BST and BTG were funded through Western Norway Health Authorities, Grant Numbers: 911809, 911852, 912171, 240222 and 912308. The funding bodies did not take part in study design, data interpretation, or writing of the manuscript. The authors wish to thank François-Xavier Legrand for helpful discussions.

Appendix A. Supplementary material

Supplementary data to this article can be found online at https://doi.org/10.1016/j.ijpharm.2021.121296.

References

Abidi, S., Bhaskara, S.M., 2003. From Chlorpromazine to Clozapine-Antipsychotic Adverse Effects and the Clinician's Dilemma. Can. J. Psych.-Revue Canadienne De Psychiatrie 48 (11), 749–755.

Administration, U.S.F.D. https://www.fda.gov/newsevents/newsroom/pressannouncements/ucm569883.htm. 2017 2018.03.28.

Agrahari, V., Agrahari, V., Mitra, A.K., 2016. Nanocarrier fabrication and macromolecule drug delivery: challenges and opportunities. Ther. Deliv. 7 (4), 257–278.

Alexis, F., Pridgen, E., Molnar, L.K., Farokhzad, O.C., 2008. Factors affecting the clearance and biodistribution of polymeric nanoparticles. Mol. Pharm. 5 (4), 505–515.

Andresen, V., Gjertsen, B.T., 2017. Drug Repurposing for the Treatment of Acute Myeloid Leukemia. Front. Med. (Lausanne) 4, 211.

Anselmo, A.C., Mitragotri, S., 2016. Nanoparticles in the clinic. Bioeng. Transl. Med. 1 (1), 10–29.

Ashburn, T.T., Thor, K.B., 2004. Drug repositioning: identifying and developing new uses for existing drugs. Nat. Rev. Drug Discov. 3 (8), 673–683.

Athanasiou, K.A., Niederauer, G.G., Agrawal, C.M., 1996. Sterilization, toxicity, biocompatibility and clinical applications of polylactic acid/polyglycolic acid copolymers. Biomaterials 17 (2), 93–102.

Avdeef, A., 2005. The rise of PAMPA. Expert Opin. Drug Metab. Toxicol. 1 (2), 325–342.

Awasthi, V.D., Garcia, D., Goins, B.A., Phillips, W.T., 2003. Circulation and biodistribution profiles of long-circulating PEG-liposomes of various sizes in rabbits. Int. J. Pharm. 253 (1-2), 121–132.

Bennion, B.J., Be, N.A., McNerney, M.W., Lao, V., Carlson, E.M., Valdez, C.A., Malfatti, M.A., Enright, H.A., Nguyen, T.H., Lightstone, F.C., Carpenter, T.S., 2017. Predicting a Drug's Membrane Permeability: A Computational Model Validated With in Vitro Permeability Assay Data. J. Phys. Chem. B 121 (20), 5228–5237.

Bicker, J., Alves, G., Fortuna, A., Falcão, A., 2014. Blood-brain barrier models and their relevance for a successful development of CNS drug delivery systems: A review. Eur. J. Pharm. Biopharm. 87 (3), 409–432.

Blair, H.A., 2018. Daunorubicin/Cytarabine Liposome: A Review in Acute Myeloid Leukaemia. Drugs 78 (18), 1903–1910.

Chen, E.C., Fathi, A.T., Brunner, A.M., 2018. Reformulating acute myeloid leukemia: liposomal cytarabine and daunorubicin (CPX-351) as an emerging therapy for secondary AML. Onco Targets Ther. 11, 3425–3434.

Chen, K.T.J., Gilabert-Oriol, R., Bally, M.B., Leung, A.W.Y., 2019. Recent Treatment Advances and the Role of Nanotechnology, Combination Products, and Immunotherapy in Changing the Therapeutic Landscape of Acute Myeloid Leukemia. Pharm. Res. 36 (9) https://doi.org/10.1007/s11095-019-2654-z.

Chen, X., Murawski, A., Patel, K., Crespi, C.L., Balimane, P.V., 2008. A novel design of artificial membrane for improving the PAMPA model. Pharm. Res. 25 (7), 1511–1520.

Cheng, J., Teply, B.A., Sherifi, I., Sung, J., Luther, G., Gu, F.X., Levy-Nissenbaum, E., Radovic-Moreno, A.F., Langer, R., Farokhzad, O.C., 2007. Formulation of functionalized PLGA-PEG nanoparticles for in vivo targeted drug delivery. Biomaterials 28 (5), 869–876.

Cornelissen, J.J., Van Putten, W.L., Verdonck, L.F., Theobald, M., Jacky, E., Daenen, S. M., van Marwijk Kooy, M., Wijermans, P., Schouten, H., Huijgens, P.C., van der Lelie, H., 2007. Results of a HOVON/SAKK donor versus no-donor analysis of myeloablative HLA-identical sibling stem cell transplantation in first remission acute myeloid leukemia in young and middle-aged adults: benefits for whom? Blood 109 (9), 3658–3666.

D'Agati, G., Beltre, R., Sessa, A., Burger, A., Zhou, Y., Mosimann, C., White, R.M., 2017. A defect in the mitochondrial protein Mpv17 underlies the transparent casper zebrafish. Dev. Biol. 430 (1), 11–17.

Danhier, F., Ansorena, E., Silva, J.M., Coco, R., Le Breton, A., Préat, V., 2012. PLGA-based nanoparticles: an overview of biomedical applications. J. Control. Release 161 (2), 505–522.

DeStefano, C.B., Hourigan, C.S., 2018. Personalizing initial therapy in acute myeloid leukemia: incorporating novel agents into clinical practice. Ther. Adv. Hematol. 9 (5), 109–121.

Di, L., Kerns, E.H., Fan, K., McConnell, O.J., Carter, G.T., 2003. High throughput artificial membrane permeability assay for blood-brain barrier. Eur. J. Med. Chem. 38 (3), 223–232.

DiNardo, C.D., Wei, A.H., 2020. How I treat acute myeloid leukemia in the era of new drugs. Blood 135 (2), 85–96.

Dinarvand, R., Sepehri, N., Manoochehri, S., Rouhani, H., Atyabi, F., 2011. Polylactide-co-glycolide nanoparticles for controlled delivery of anticancer agents. Int J Nanomed. 6, 877–895.

Döhner, H., Estey, E.H., Amadori, S., Appelbaum, F.R., Büchner, T., Burnett, A.K., Dombret, H., Fenaux, P., Grimwade, D., Larson, R.A., Lo-Coco, F., 2010. Diagnosis and management of acute myeloid leukemia in adults: recommendations from an international expert panel, on behalf of the European LeukemiaNet. Blood 115 (3), 453–474.

Döhner, H., Estey, E., Grimwade, D., Amadori, S., Appelbaum, F.R., Büchner, T., Dombret, H., Ebert, B.L., Fenaux, P., Larson, R.A., Levine, R.L., 2017. Diagnosis and management of AML in adults: 2017 ELN recommendations from an international expert panel. Blood 129 (4), 424–447.

Drug database (Chlorpromazine): http://www.drugs.com/ppa/chlorpromazine.html (Last accessed: 03.04.2019).

Drug database (Chlorpromazine): http://www.drugbank.ca/drugs/DB00477. Last accessed: 25.05.2018.

Duarte, D., Hawkins, E.D., Akinduro, O., Ang, H., De Filippo, K., Kong, I.Y., Haltalli, M., Ruivo, N., Straszkowski, L., Vervoort, S.J., McLean, C., Weber, T.S., Khorshed, R., Pirillo, C., Wei, A., Ramasamy, S.K., Kusumbe, A.P., Duffy, K., Adams, R.H., Purton, L.E., Carlin, L.M., Lo Celso, C., 2018. Inhibition of Endosteal Vascular Niche Remodeling Rescues Hematopoietic Stem Cell Loss in AML. Cell Stem Cell 22 (1), 64–77.e6.

Dutta, D., Donaldson, J.G., 2012. Search for inhibitors of endocytosis: Intended specificity and unintended consequences. Cell Logist 2 (4), 203–208.

Estey, E., Döhner, H., 2006. Acute myeloid leukaemia. Lancet 368 (9550), 1894–1907.

Evensen, L., Johansen, P.L., Koster, G., Zhu, K., Herfindal, L., Speth, M., Fenaroli, F., Hildahl, J., Bagherifam, S., Tulotta, C., Prasmickaite, L., Mælandsmo, G.M., Snaar-Jagalska, E., Griffiths, G., 2016. Zebrafish as a model system for characterization of nanoparticles against cancer. Nanoscale 8 (2), 862–877.

Fernandez, H.F., Sun, Z., Yao, X., Litzow, M.R., Luger, S.M., Paietta, E.M., Racevskis, J., Dewald, G.W., Ketterling, R.P., Bennett, J.M., Rowe, J.M., Lazarus, H.M., Tallman, M.S., 2009. Anthracycline dose intensification in acute myeloid leukemia. N. Engl. J. Med. 361 (13), 1249–1259.

Ferrari, R., Sponchioni, M., Morbidelli, M., Moscatelli, D., 2018. Polymer nanoparticles for the intravenous delivery of anticancer drugs: the checkpoints on the road from the synthesis to clinical translation. Nanoscale 10 (48), 22701–22719.

Fleming, A., Diekmann, H., Goldsmith, P., 2013. Functional characterisation of the maturation of the blood-brain barrier in larval zebrafish. PLoS One 8 (10), e77548.

Fonseca-Santos, B., Gremiao, M.P.D., Chorilli, M., 2015. Nanotechnology-based drug delivery systems for the treatment of Alzheimer's disease. Int. J. Nanomed. 10.

Fredenberg, S., Wahlgren, M., Reslow, M., Axelsson, A., 2011. The mechanisms of drug release in poly(lactic-co-glycolic acid)-based drug delivery systems–a review. Int. J. Pharm. 415 (1-2), 34–52.

Gausdal, G., Gjertsen, B.T., McCormack, E., Van Damme, P., Hovland, R., Krakstad, C., Bruserud, Ø., Gevaert, K., Vandekerckhove, J., Døskeland, S.O., 2008. Abolition of stress-induced protein synthesis sensitizes leukemia cells to anthracycline-induced death. Blood 111 (5), 2866–2877.

Gelebart, P., Popa, M., McCormack, E., 2015. Xenograft Models of Primary Acute Myeloid Leukemia for the Development of Imaging Strategies and Evaluation of Novel Targeted Therapies. Curr. Pharm. Biotechnol. 17 (1), 42–51.

Gupta, S.C., Sung, B., Prasad, S., Webb, L.J., Aggarwal, B.B., 2013. Cancer drug discovery by repurposing: teaching new tricks to old dogs. Trends Pharmacol. Sci. 34 (9), 508–517.

Haag, P., Zielinska-Chomej, K., Juntti, T., Kanter, L., Lewensohn, R., Stenke, L., Viktorsson, K., 2013. Phenothiazines induce cytotoxicity and enhance chemotherapy-induced cell death signaling in acute myeloid leukemia. Mol. Cancer Therapeut. 12 (11).

Halayqa, M., Domanska, U., 2014. PLGA biodegradable nanoparticles containing perphenazine or chlorpromazine hydrochloride: effect of formulation and release. Int. J. Mol. Sci. 15 (12), 23909–23923.

Hanusova, V., Skalova, L., Kralova, V., Matouskova, P., 2015. Potential anti-cancer drugs commonly used for other indications. Curr Cancer Drug Targets 15 (1), 35–52.

Ito, T., Handa, H., 2015. MYELOID DISEASE Another action of a thalidomide derivative. Nature 523 (7559), 167–168.

Jin, G., Wong, S.T.C., 2014. Toward better drug repositioning: prioritizing and integrating existing methods into efficient pipelines. Drug Discov. Today 19 (5), 637–644.

Kamaly, N., Yameen, B., Wu, J., Farokhzad, O.C., 2016. Degradable controlled-release polymers and polymeric nanoparticles: mechanisms of controlling drug release. Chem. Rev. 116 (4), 2602–2663.

Kansy, M., Senner, F., Gubernator, K., 1998. Physicochemical high throughput screening: parallel artificial membrane permeation assay in the description of passive absorption processes. J. Med. Chem. 41 (7), 1007–1010.

Kimmel, C.B., Ballard, W.W., Kimmel, S.R., Ullmann, B., Schilling, T.F., 1995. Stages of embryonic development of the zebrafish. Dev. Dyn. 203 (3), 253–310.

Kohlschütter, J., Michelfelder, S., Trepel, M., 2008. Drug delivery in acute myeloid leukemia. Expert. Opin. Drug Deliv. 5 (6), 653–663.

Kolakowska, T., Wiles, D.H., Gelder, M.G., McNeilly, A.S., 1976. Clinical significance of plasma chlorpromazine levels. II. Plasma levels of the drug, some of its metabolites and prolactin in patients receiving long-term phenothiazine treatment. Psychopharmacology (Berl) 49 (1), 101–107.

Kolakowska, T., Orr, M., Gelder, M., Heggie, M., Wiles, D., Franklin, M., 1979. Clinical significance of plasma drug and prolactin levels during acute chlorpromazine treatment: a replication study. Br. J. Psych. 135 (4), 352–359.

Kumar, B., Chen, C.C., 2018. Acute myeloid leukemia remodels endosteal vascular niche into a leukemic niche. Stem Cell Investig. 5, 34.

Leitch, C., Osdal, T., Andresen, V., Molland, M., Kristiansen, S., Nguyen, X.N., Bruserud, Ø., Gjertsen, B.T., McCormack, E., 2016. Hydroxyurea synergizes with valproic acid in wild-type p53 acute myeloid leukaemia. Oncotarget 7 (7), 8105–8118.

Lichtman, M.A., 2013. A historical perspective on the development of the cytarabine (7days) and daunorubicin (3days) treatment regimen for acute myelogenous leukemia: 2013 the 40th anniversary of 7+3. Blood Cells Mol. Dis. 50 (2), 119–130.

Longo, D.L., Döhner, H., Weisdorf, D.J., Bloomfield, C.D., 2015. Acute Myeloid Leukemia. N. Engl. J. Med. 373 (12), 1136–1152.

Makadia, H.K., Siegel, S.J., 2011. Poly Lactic-co-Glycolic Acid (PLGA) as Biodegradable Controlled Drug Delivery Carrier. Polymers (Basel) 3 (3), 1377–1397.

Malam, Y., Loizidou, M., Seifalian, A.M., 2009. Liposomes and nanoparticles: nanosized vehicles for drug delivery in cancer. Trends Pharmacol. Sci. 30 (11), 592–599.

Matsuo, Y., MacLeod, R.A.F., Uphoff, C.C., Drexler, H.G., Nishizaki, C., Katayama, Y., Kimura, G., Fujii, N., Omoto, E., Harada, M., Orita, K., 1997. Two acute monocytic leukemia (AML-M5a) cell lines (MOLM-13 and MOLM-14) with interclonal phenotypic heterogeneity showing MLL-AF9 fusion resulting from an occult chromosome insertion, ins(11;9)(q23;p22p23). Leukemia 11 (9), 1469–1477.

McCabe, B., Liberante, F., Mills, K.I., 2015. Repurposing medicinal compounds for blood cancer treatment. Ann. Hematol. 94 (8), 1267–1276.
McClelland, G.R., Cooper, S.M., Pilgrim, A.J., 1990. A comparison of the central nervous system effects of haloperidol, chlorpromazine and sulpiride in normal volunteers. Br. J. Clin. Pharmacol. 30 (6), 795–803.
McCormack, E., Haaland, I., Venås, G., Forthun, R.B., Huseby, S., Gausdal, G., Knappskog, S., Micklem, D.R., Lorens, J.B., Bruserud, Ø., Gjertsen, B.T., 2012. Synergistic induction of p53 mediated apoptosis by valproic acid and nutlin-3 in acute myeloid leukemia. Leukemia 26 (5), 910–917.
Mensch, J., Melis, A., Mackie, C., Verreck, G., Brewster, M.E., Augustijns, P., 2010. Evaluation of various PAMPA models to identify the most discriminating method for the prediction of BBB permeability. Eur. J. Pharm. Biopharm. 74 (3), 495–502.
Michalak, K., Wesolowska, O., Motohashi, N., Molnar, J., Hendrich, A.B., 2006. Interactions of phenothiazines with lipid bilayer and their role in multidrug resistance reversal. Current Drug Targets 7 (9), 1095–1105.
Midha, K.K., Hawes, E.M., Hubbard, J.W., Korchinski, E.D., McKay, G., 1989. Intersubject variation in the pharmacokinetics of chlorpromazine in healthy men. J Clin Psychopharmacol 9 (1), 4–8.
Moghimi, S.M., 1995. Exploiting bone-marrow microvascular structure for drug-delivery and future therapies. Adv. Drug Deliv. Rev. 17 (1), 61–73.
Myhren, L., Nilssen, I.M., Nicolas, V., Døskeland, S.O., Barratt, G., Herfindal, L., 2014. Efficacy of multi-functional liposomes containing daunorubicin and emetine for treatment of acute myeloid leukaemia. Eur. J. Pharm. Biopharm. 88 (1), 186–193.
Nair, L.S., Laurencin, C.T., 2007. Biodegradable polymers as biomaterials. Prog. Polym. Sci. 32 (8-9), 762–798.
Narvekar, M., Xue, H.Y., Eoh, J.Y., Wong, H.L., 2014. Nanocarrier for Poorly Water-Soluble Anticancer Drugs-Barriers of Translation and Solutions. Aaps Pharmscitech 15 (4), 822–833.
Panyam, J., Labhasetwar, V., 2003. Biodegradable nanoparticles for drug and gene delivery to cells and tissue. Adv. Drug Deliv. Rev. 55 (3), 329–347.
Parveen, S., Misra, R., Sahoo, S.K., 2012. Nanoparticles: a boon to drug delivery, therapeutics, diagnostics and imaging. Nanomedicine 8 (2), 147–166.
Pinto Reis, C., Neufeld, R.J., Ribeiro, A.J., Veiga, F., 2006. Methods for preparation of drug-loaded polymeric nanoparticles. Nanomed.-Nanotechnol. Biol. Med. 2 (1), 8–21.
Quentmeier, H., Reinhardt, J., Zaborski, M., Drexler, H.G., 2003. FLT3 mutations in acute myeloid leukemia cell lines. Leukemia 17 (1), 120–124.
Quiñonez-Silvero, C., Hübner, K., Herzog, W., 2020. Development of the brain vasculature and the blood-brain barrier in zebrafish. Dev. Biol. 457 (2), 181–190.
Quintanar-Guerrero, D., Allémann, E., Fessi, H., Doelker, E., 1998. Preparation techniques and mechanisms of formation of biodegradable nanoparticles from preformed polymers. Drug Dev. Ind. Pharm. 24 (12), 1113–1128.
Rabanel, J.-M., Hildgen, P., Banquy, X., 2014. Assessment of PEG on polymeric particles surface, a key step in drug carrier translation. J. Control. Release 185, 71–87.
W.S. Rasband, ImageJ. U. S. National Institutes of Health, Bethesda, Maryland, USA. http://imagej.nih.gov/ij/, 1997-2016.
Rejman, J., Oberle, V., Zuhorn, I.S., Hoekstra, D., 2004. Size-dependent internalization of particles via the pathways of clathrin-and caveolae-mediated endocytosis. Biochem. J. 377, 159–169.
Rosowski, E.E., 2020. Determining macrophage versus neutrophil contributions to innate immunity using larval zebrafish. Dis. Model Mech. 13 (1).
Rowe, J.M., 2013. Important milestones in acute leukemia in 2013. Best Pract. Res. Clin. Haematol. 26 (3), 241–244.
Rowe, J., Tallman, M., 2010. How I treat acute myeloid leukemia. Blood 116 (17), 3147–3156.
Sachlos, E., Risueño, R.M., Laronde, S., Shapovalova, Z., Lee, J.H., Russell, J., Malig, M., McNicol, J.D., Fiebig-Comyn, A., Graham, M., Levadoux-Martin, M., 2012. Identification of drugs including a dopamine receptor antagonist that selectively target cancer stem cells. Cell 149 (6), 1284–1297.
Sah, H., Thoma, L.A., Desu, H.R., Sah, E., Wood, G.C., 2013. Concepts and practices used to develop functional PLGA-based nanoparticulate systems. Int. J. Nanomedicine 8, 747–765.
Sahay, G., Alakhova, Da.Y., Kabanov, A.V., 2010. Endocytosis of nanomedicines. J. Control. Release 145 (3), 182–195.
Sarin, H., 2010. Physiologic upper limits of pore size of different blood capillary types and another perspective on the dual pore theory of microvascular permeability. J. Angiogenes Res. 2, 14.
Sauvage, F., Barratt, G., Herfindal, L., Vergnaud-Gauduchon, J., 2015. The use of nanocarriers in acute myeloid leukaemia therapy: challenges and current status. Curr. Pharm. Biotechnol. 17 (1), 30–41.
Sauvage, F., Fattal, E., Al-Shaer, W., Denis, S., Brotin, E., Denoyelle, C., Blanc-Fournier, C., Toussaint, B., Messaoudi, S., Alami, M., Barratt, G., Vergnaud-Gauduchon, J., 2018. Antitumor activity of nanoliposomes encapsulating the novobiocin analog 6BrCaQ in a triple-negative breast cancer model in mice. Cancer Lett. 432, 103–111.
Schindelin, J., Arganda-Carreras, I., Frise, E., Kaynig, V., Longair, M., Pietzsch, T., Preibisch, S., Rueden, C., Saalfeld, S., Schmid, B., Tinevez, J.-Y., White, D.J., Hartenstein, V., Eliceiri, K., Tomancak, P., Cardona, A., 2012. Fiji: an open-source platform for biological-image analysis. Nat. Methods 9 (7), 676–682.
Schneider, C.A., Rasband, W.S., Eliceiri, K.W., 2012. NIH Image to ImageJ: 25 years of image analysis. Nat. Methods 9 (7), 671–675.
Singh, A., Myklebust, N.N., Furevik, S.M.V., Haugse, R., Herfindal, L., 2019. Immunoliposomes in acute myeloid leukaemia therapy: an overview of possible targets and obstacles. Curr. Med. Chem. 26 (28), 5278–5292.
Soica, C., Oprean, C., Borcan, F., Danciu, C., Trandafirescu, C., Coricovac, D., Crăiniceanu, Z., Dehelean, C.A., Munteanu, M., 2014. The synergistic biologic activity of oleanolic and ursolic acids in complex with hydroxypropyl-gamma-cyclodextrin. Molecules 19 (4), 4924–4940.
Solaro, R., Chiellini, F., Battisti, A., 2010. Targeted Delivery of Protein Drugs by Nanocarriers. Materials 3 (3), 1928–1980.
Song, C.X., Labhasetwar, V., Murphy, H., Qu, X., Humphrey, W.R., Shebuski, R.J., Levy, R.J., 1997. Formulation and characterization of biodegradable nanoparticles for intravascular local drug delivery. J. Control. Release 43 (2-3), 197–212.
Sou, K., Goins, B., Takeoka, S., Tsuchida, E., Phillips, W.T., 2007. Selective uptake of surface-modified phospholipid vesicles by bone marrow macrophages in vivo. Biomaterials 28 (16), 2655–2666.
Steins, M.B., Bieker, R., Padró, T., Kessler, T., Kienast, J., Berdel, W.E., Mesters, R.M., 2003. Thalidomide for the treatment of acute myeloid leukemia. Leuk. Lymphoma 44 (9), 1489–1493.
Stone, R.M., 2017. Which new agents will be incorporated into frontline therapy in acute myeloid leukemia? Best Pract. Res. Clin. Haematol. 30 (4), 312–316.
Suk, J.S., Xu, Q., Kim, N., Hanes, J., Ensign, L.M., 2016. PEGylation as a strategy for improving nanoparticle-based drug and gene delivery. Adv. Drug Deliv. Rev. 99, 28–51.
Svenson, S., 2014. What nanomedicine in the clinic right now really forms nanoparticles? Wiley Interdiscip. Rev. Nanomed. Nanobiotechnol. 6 (2), 125–135.
Thing Mortensen, B., Østrup Jensen, P., Helledie, N., Ole Iversen, P., RalfkiAER, E., Knud Larsen, J., Thorup Madsen, M., 1998. Changing bone marrow micro-environment during development of acute myeloid leukaemia in rats. Br. J. Haematol. 102 (2), 458–464.
Uhrich, K.E., Cannizzaro, S.M., Langer, R.S., Shakesheff, K.M., 1999. Polymeric systems for controlled drug release. Chem. Rev. 99 (11), 3181–3198.
Wahlin, A., Markevärn, B., Golovleva, I., Nilsson, M., 2002. Improved outcome in adult acute myeloid leukemia is almost entirely restricted to young patients and associated with stem cell transplantation. Eur. J. Haematol. 68 (1), 54–63.
Walkey, C.D., Olsen, J.B., Guo, H., Emili, A., Chan, W.C.W., 2012. Nanoparticle size and surface chemistry determine serum protein adsorption and macrophage uptake. J. Am. Chem. Soc. 134 (4), 2139–2147.
White, .T., Saxena, M.T., Mumm, J.S., 2019. Let's get small (and smaller): Combining zebrafish and nanomedicine to advance neuroregenerative therapeutics. Adv. Drug Deliv. Rev. 148, 344–359.
White, R.M., Sessa, A., Burke, C., Bowman, T., LeBlanc, J., Ceol, C., Bourque, C., Dovey, M., Goessling, W., Burns, C.E., Zon, L.I., 2008. Transparent adult zebrafish as a tool for in vivo transplantation analysis. Cell Stem Cell 2 (2), 183–189.
Whitehead, K.A., Langer, R., Anderson, D.G., 2009. Knocking down barriers: advances in siRNA delivery. Nat. Rev. Drug Discov. 8 (2), 129–138.
Wicki, A., Witzigmann, D., Balasubramanian, V., Huwyler, J., 2015. Nanomedicine in cancer therapy: challenges, opportunities, and clinical applications. J. Control. Release 200, 138–157.
Wode-Helgodt, B., Alfredsson, G., 1981. Concentrations of chlorpromazine and two of its active metabolites in plasma and cerebrospinal fluid of psychotic patients treated with fixed drug doses. Psychopharmacology 73 (1), 55–62.
Xu, P., Gullotti, E., Tong, L., Highley, C.B., Errabelli, D.R., Hasan, T., Cheng, J.-X., Kohane, D.S., Yeo, Y., 2009. Intracellular drug delivery by poly(lactic-co-glycolic acid) nanoparticles, revisited. Mol. Pharm. 6 (1), 190–201.
Zhao, Y., GAO, J., Ji, J., Gao, M., Yin, Q., Qiu, Q., Wang, C., Chen, S., Xu, J., Liang, R., Cai, Y., Wang, X., 2014. Cytotoxicity enhancement in MDA-MB-231 cells by the combination treatment of tetrahydropalmatine and berberine derived from Corydalis yanhusuo W T. Wang. J. Intercult. Ethnopharmacol. 3 (2), 68. https://doi.org/10.5455/jice:10.5455/jice:20140123040224.
Zhelev, Z., Ohba, H., Bakalova, R., Hadjimitova, V., Ishikawa, M., Shinohara, Y., Baba, Y., 2004. Phenothiazines suppress proliferation and induce apoptosis in cultured leukemic cells without any influence on the viability of normal lymphocytes - Phenothiazines and leukemia. Cancer Chemother. Pharmacol. 53 (3), 267–275.